1

Introduction to Single-Molecule Magnets

Małgorzata Hołyńska

Philipps University Marburg, Department of Chemistry, Hans-Meerwein Straße, 35043 Marburg, Germany

Highlights

This chapter will answer the following questions:

- What are single-molecule magnets (SMMs)?
- What are the related materials – single-chain magnets, single-ion magnets, single-toroid magnets?
- What is the history of SMMs?
- What applications are possible?
- What are the general and recent trends in SMM science?

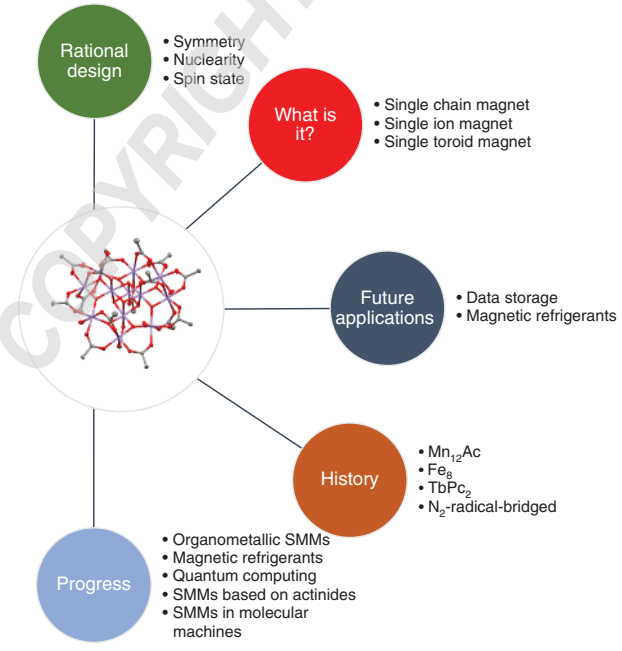

Mind-map summary of this chapter.

Single-Molecule Magnets: Molecular Architectures and Building Blocks for Spintronics,
First Edition. Edited by Małgorzata Hołyńska.

1.1 What Is a Single-Molecule Magnet?

We will start with a definition crucial to the whole book, namely of that of a single-molecule magnet (SMM). The term is self-explanatory, meaning a single molecule which is a magnet. But what does it take to be a magnet? Normally, we consider bulk magnets, e.g. materials in which the magnetic moment stems from the presence of unpaired electrons. Their spins tend to form parallel/antiparallel arrangements within areas called domains, separated by the so-called Bloch walls. The currently known most powerful "classical" magnets include $SmCo_5$ and $Nd_2Fe_{14}B$. On the other hand, if we consider SMMs, we must assume that a single molecule is a "magnetic domain." The molecule can be magnetized and the attained magnetization relaxes slowly on removal of the external magnetic field. This new concept of molecular magnetism has experimental consequences, such as out-of-phase signals in ac studies of the magnetic properties. A detailed discussion of these will be included in Chapter 2 while an overview of the basic knowledge of them is addressed in this chapter. The unusual quantum phenomena found in SMMs open the possibilities of unprecedented applications, e.g. in molecular spintronics/quantum computing. These applications will also be reviewed in the following sections, underlining the interdisciplinary character of SMM science.

As the famous physicist Richard Feynman stated, "there's plenty of room at the bottom." "Bottom" is the world of atoms and molecules, also magnetic molecules being SMMs. Starting with this "bottom" to create a magnetic material represents the so-called "bottom-up" approach [1]. On the other hand, magnetic macromaterials, such as Prussian blue, may be taken to the "bottom" as a result of a "top-down" approach [2].

Molecular architecture is the key to understanding the magnetic properties of SMMs; therefore, X-ray diffraction studies have played a crucial role in the characterization of SMMs and require optimization of their synthesis/crystallization conditions, as reviewed in Chapter 2. Gaining insight into their magnetic properties through superconducting quantum interference device (SQUID) magnetometry or electron paramagnetic resonance (EPR) studies requires theoretical interpretation and often advanced computations, as described in Chapters 3 and 4. Further characterization methods include paramagnetic nuclear magnetic resonance (NMR), magnetic circular dichroism or, in special cases, Mössbauer spectroscopy, as described in Chapter 5.

There are other magnetically interesting molecules related to SMMs, such as single-chain magnets (SCMs), single-ion magnets (SIMs), and single-toroid magnets (STMs). These materials will be briefly described in the next three sections. In addition, there will be some brief explanation of possible future applications and how they could work.

1.1.1 Single-Chain Magnets (SCMs)

SCMs comprise ferromagnetic chain-like molecules that do not interact magnetically with each other. The modeling of their magnetic properties is different

than that for SMMs: classical spin Heisenberg chain or Ising chain equations finds application in this case.

The first prediction of SCM behavior based on their magnetic properties was published by Glauber in 1963 [3]. The possibility of slow relaxation of magnetization in zero-dimensional systems was postulated. The necessary conditions to enable this phenomenon are:

- $J/J' > 10^4$ (where J describes the magnetic interaction within the chain and J' between the chains),
- 1D Ising ferromagnetism or ferrimagnetism.

After coining the term SMM in the 1990s, Gatteshi and coworkers [4] were the first researchers to show that these conditions could be realized experimentally. They demonstrated this by using the example of a coordination polymer comprising $Co(hfac)_2$ and radical (NITPhOMe = 4′-methoxy-phenyl-4,4,5,5-tetramethylimidazoline-1-oxyl-3-oxide) moieties. The polymeric chains behaved as 1D ferrimagnets with the easy axis of magnetization along their trigonal axis and slow relaxation of magnetization. On the other hand, these properties could not be found in the manganese(II) analogue and it was also proven that they could not result from a spin glass behavior or 3D ordering.

Interestingly, SCMs can be constructed from SMMs. A good example is the first strategy applied to organize ferromagnetic SMMs into 1D chains as reported by Clérac and coworkers [5] The applied building blocks were Mn^{III}–Ni^{II}–Mn^{III} linear trinuclear complexes, $[Mn_2(5\text{-Rsaltmen})_2Ni(pao)_2(phen)](ClO_4)_2$ (where R = Cl or Br, $Rsaltmen^{2-}$ = *N,N′*-(1,1,2,2-tetramethyl-ethylene)bis(5-R-salicylideneiminate). The SMM properties of these compounds, with ground state of $S = 3$ and uniaxial magnetic anisotropy around ~2.4 K, play a crucial role in the theoretical description of the resulting SCMs.

Currently, a common strategy applied to obtain SCMs is the synthesis of metal – bulky radical chains where large organic substituents help to isolate the chains magnetically. Three options are recommended: ferromagnetic, ferrimagnetic, or spin-canted chains [6].

In recent years, much progress has been noted in SCM science. A review covering the progress until 2014 was published by Brooker and coworkers [7].

Cassaro, Vaz et al. [8] reported on SCMs with a very high blocking temperature of ~13.2 K and a very high coercive field of 49 kOe at 4.0 K for one of them. The compounds are based on metal (Mn^{II} or Co^{II}) hexafluoroacetylacetonates and NaphNN (1-naphthyl nitronylnitroxide) radicals. The remarkably high values of the relevant properties were detected in the Co^{II} complex.

Zhang, Wang, Song, and coworkers [9] synthesized SCMs based on octacyanotungstate with highest energy barriers for cyanide compounds of 252(9) and 224(7) K for $(Ph_4P)[Co^{II}(3\text{-Mepy})_{2.7}(H_2O)_{0.3}W^{V}(CN)_8]\cdot 0.6H_2O$, and $(Ph_4As)[Co^{II}(3\text{-Mepy})_3W^{V}(CN)_8]$ (2,3-Mepy = 3-methylpyridine), respectively.

The use of such cyanometalate complexes is very promising due to the possibility to construct coordination polymers and also because it is available for many metals in different oxidation states. Even quite unstable building blocks such as $[Mn(CN)_6]^{3-}$ can be used: Dunbar and coworkers reported on an SCM

$\{[(tptz)Mn^{II}(H_2O)Mn^{III}(CN)_6]_2Mn^{II}(H_2O)_2\}_n \cdot 4n\,MeOH{\cdot}2n\,H_2O$ (tptz = 2,4,6-tri(2-pyridyl)-1,3,5-triazine) with an energy barrier of 40.5(7) K [10].

1.1.2 Single-Ion Magnets (SIMs)

In the case of single-ion magnets (SIMs or SIMMs – single-ion molecular magnets or MSMM – mononuclear single-molecule magnets) the magnetic properties are governed by a single ion, without direct coupling to any other magnetic centers. Here, particularly suitable building blocks are Dy^{3+}, Tb^{3+}, or Ho^{3+}due to their high-spin ground state and unquenched orbital angular momentum, resulting in high magnetic anisotropy.

In such simple systems the first significant progress in increasing the energy barrier was achieved with the introduction of Ishikawa's "double-decker" bis(phthalocyaninato)lanthanide ions [11].

Recently, SIMs were found also in 3d metal and actinide complexes. From examples of these materials it became evident how small changes in the central metal ion coordination environment can impact the magnetic properties. The main problem in enhancing the lanthanide-based SIMs turned out to be the quantum tunneling of magnetization.

The first endohedral SMM, $DySc_2N@C_{80}$, was reported by Greber and coworkers [12]. A single Dy^{3+} ion was encapsulated in a diamagnetic carbon cage along with two Sc^{3+} ions and nitride counterions. Its ground state could be stabilized by the ligand field. By a combination of element-specific X-ray magnetic circular dichroism (XMCD) and SQUID magnetometry the SMM behavior of this compound was shown to originate from the single Dy^{3+} ion. Especially for the magnetically diluted samples, very high relaxation times were reported at zero field and magnetization hysteresis loops were recorded under 6 K. Recently, the same group contributed to a study of $DySc_2N@C_{80}$ molecules deposited on a metal surface. A rhodium (111) substrate was chosen and X-ray absorption spectroscopy (XAS) was employed to prove the alignment of the magnetic moments on this surface for the investigated SMM.

The breakthrough in the introduction of SIMs based on 3d metals was achieved in 2013 with the report on an unstable linear iron(I) complex, $[K(crypt\text{-}222)][Fe(C(SiMe_3)_3)_2]$, by Long and coworkers [13]. In spite of the seemingly unfavorable odds in comparison to lanthanides (lower spin-orbit coupling constants, the possibility that strong coupling of the d-orbitals to the ligand field may quench first-order orbital contributions to the magnetic moment) many new 3d-metal-based systems acting as SIMs followed [14]. These include Mn(III) [15–17], Co(II) [18–25], Ni(I) [26], Ni(II) [27, 28], or Cr(II) complexes [29]. An excellent overview of the recent achievements in this field as well as its future directions were provided by Murugesu and coworkers [14]. Among the future trends, the synthesis of 4d/5d-metal complexes, e.g. Re(IV), is listed. 4d/5d metal orbitals are expected to be involved in stronger exchange interactions due to their increased radial extension.

Ruiz, Clérac, Smith and coworkers [30] showed that SMM behavior can be detected even in a mononuclear, low-spin Mn(IV) (d^3, $S_T = 1/2$) complex $PhB(MesIm)_3Mn{\equiv}N$ with tris(carbine)borate capping ligand. Owing to

degenerate electron configuration a Jahn–Teller distortion was observed in this four-coordinate Mn(IV) complex, which was fully rationalized with electronic structure calculations. It was demonstrated that the slow relaxation of magnetization under an applied dc field in this case is dominated by quantum tunneling mechanism (QTM)/Raman mechanism, but that no Orbach contribution is possible. In order to limit the QTM part enhanced by the Jahn–Teller distortion, future efforts would address related complexes with less structural deformation to possibly increase the relaxation times.

Liu, Chibotaru, Wernsdorfer et al. continued their search for SIMs in the lanthanide complexes, which led to a new high magnetization reversal barrier of over 1000 K with magnetic loops up to 14 K [31]. These remarkable properties were found in air- and heat-stable [Dy(bbpen)X] complexes (X = Cl or Br, H_2bbpen = *N*,*N*′-bis(2-hydroxybenzyl)-*N*,*N*′-bis(2-methylpyridyl)ethylenediamine)) of a D_{5h} symmetry. The magnetization relaxation pathway for these compounds was investigated in detail both experimentally and theoretically, leading to the involvement of the second excited Kramers doublet or the third excited state. These were assumed to result from an interplay between a strong axial crystal field and a weaker transverse crystal field. On the other hand, the majority of known lanthanide-based SIMs favor relaxation through the first excited $\pm M_J$ state. An important molecular feature governing this turned out to be the symmetry with two closely spaced axial ligands and five distant equatorial ligands. The closer to the ideal D_{5h} case, the higher was the energy barrier. Thus, quite specific rules were proposed to be pursued in the future.

Chilton, Winpenny, Zheng, and coworkers recently reported on a monometallic dysprosium complex $[Dy(O^tBu)_2(py)_5][BPh_4]$ with a record magnetization reversal barrier of 1815(1) K and a blocking temperature of 14 K [32]. These outstanding values are achieved by focussing on a strong axial ligand field with the alkoxy ligands in axial position and weak py ligands in equatorial position and with the use of a D_{5h} symmetry.

1.1.3 Single-Toroid Magnets (STMs)

A special case of magnets related to SMMs are STMs or single-molecule toroics, SMTs). The concept of STMs was introduced by Chibotaru et al. [33]. These molecules are bistable and display a toroidal magnetic state that is detectable in single-crystal magnetic studies. A prominent example of this so far small group of compounds are dysprosium(III) complexes with a toroidal arrangement of the local easy axes and non-magnetic ground state [34]. Potential applications of STMs are, e.g. in quantum computing, as multiferroic materials or for magnetic cooling. In data storage, SMTs are expected to be even more efficient than SMMs due to a slower decay of the magnetic field produced by the net toroidal moment [34].

In 2014, Tang and coworkers provided an overview of STMs in Ising-type lanthanide molecular clusters [34]. The toroidal moment was stated to arise from a vortex arrangement of local magnetic moments owing to a wheel-like arrangement and specific interactions involving the magnetic centers. STMs should be insensitive to homogeneous magnetic fields and manipulable with

electrical fields. The examples of STMs reported so far include a heterometallic 1D [$CuDy_3$] coordination polymer [35], a planar [Dy_4] complex [36], more triangular [Dy_3] complexes, or a wheel-like [Dy_6] complex. Tang and coworkers classified them into the following four groups:

- net toroidal moment STMs (toroidal magnetic state in the absence of a total magnetic moment, e.g. the planar complex [$Dy_4(\mu_3\text{-}OH)_2(\mu\text{-}OH)_2(2,2\text{-bpt})_4(NO_3)_4(EtOH)_2$], where 2,2-bptH = 3,5-bis(pyridin-2-yl)-1,2,4-triazole) [36],
- mixed-moment STMs (the conventional magnetic moments are not canceled out due to low molecular symmetry, e.g. [$Dy_3(\mu_3\text{-}OH)_2L_3Cl(H_2O)_5]Cl_3$, where HL = *o*-vanillin [37],
- zero-toroidal moment compounds (the toroidal moments of the constituent structural units cancel out, e.g. the coordination polymer [$Cu(Val)_2CH_3OH][L_3Dy_3(\mu_3\text{-}OH)_2(NO_3)_4]_n$, where HL = *o*-vanillin, Val = valine [35],
- enhanced toroidal moment compounds (enhanced toroidal moment due to ferromagnetic coupling of the toroidal moments of the constituent units, e.g. [$Dy_6L_4(\mu_4\text{-}O)(NO_3)_4(CH_3OH)]\cdot CH_3OH$, where H_3L = 2,6-bis((2-hydroxyethylimino)methyl)-4-methylphenol [38].

These toroidal moments are influenced by molecular symmetry, metal ions coordination environment, or the bridging ligands transmitting exchange coupling interactions that are regarded as crucial elements for the design of STMs.

Tang, Le Guennic, Shi et al. in their pursuit of STMs decided to focus on triangular [Dy_3] units and manipulation of the terminal ligand, also in terms of charge. This way, SMM behavior and toroidal magnetic moment governed by the arrangement of the local easy axes could be induced simultaneously. Thus, a toroidal magnetic moment was observed in a [$Dy_6L_2(\mu_3\text{-}OH)_4(\mu_2\text{-}OH)_2(H_2O)_{12}]_8Br\cdot 2CH_3CN\cdot 6CH_3OH$ complex with only neutral terminal ligands. When these neutral ligands are replaced by charged ligands, such as thiocyanates or nitrates, the toroidal moment disappears. The result was rationalized with high-level computational methods and underlined the role of ancilliary ligands in the design of STMs.

1.2 Historical Aspects

Before embarking on an overview of the recent progresses made in SMM science, we will focus on the historical aspects that help to have a better understanding of the present state of the art (Figure 1.1). The first compound for which SMM behavior was reported was a dodecanuclear mixed-valence [Mn_{12}] complex [39]. A simple system of the reaction of Mn^{2+} with MnO_4^- ions in acetic and propionic acids yielded a crystalline product that was assigned the formula [$Mn_{12}(CH_3COO)_{16}(H_2O)_4O_{12}]\cdot 2CH_3COOH\cdot 4H_2O$ based on full crystal structure determination with X-ray diffraction studies and wet chemical analysis. However, the possibility of this formation was already mentioned by Weinland & Fischer in 1921 [40].

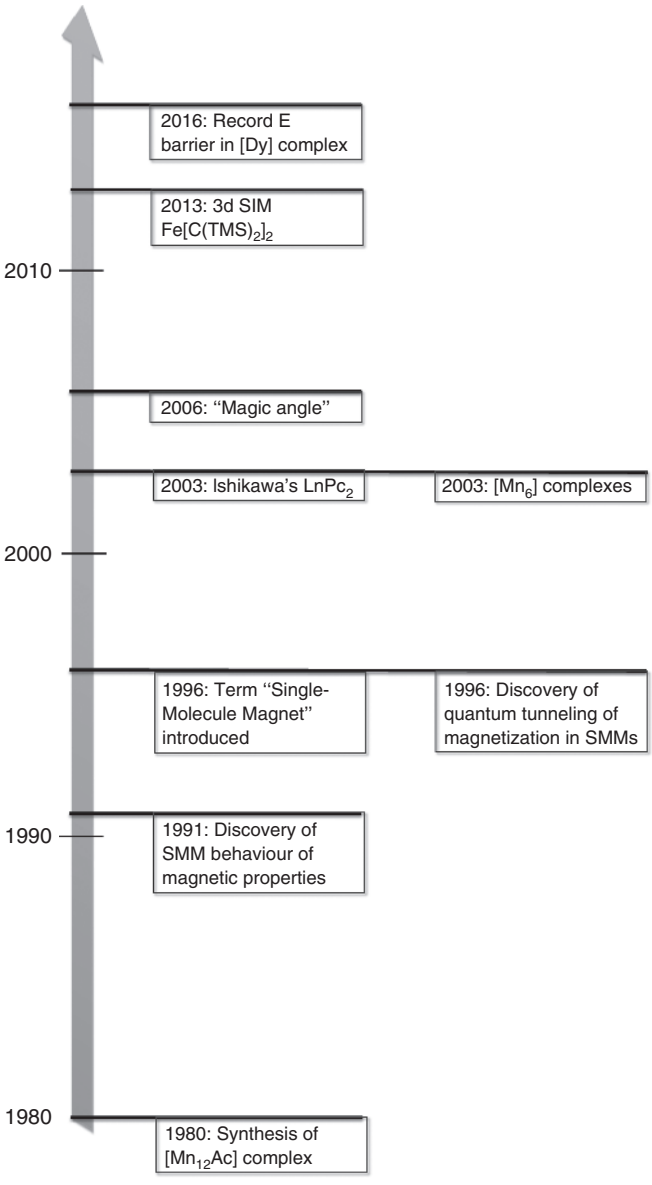

Figure 1.1 Selected milestones in the history of SMMs.

In the complex molecule (Figure 1.2Aa) of an S_4 symmetry, a central cube of four Mn^{4+} ions bridged by oxo ligands is interconnected to an outer ring of eight Mn^{3+} ions bridged by oxo- and acetate ligands. The coordination spheres of the Mn atoms are completed with terminal water ligands.

Routine studies of the magnetic properties performed with a Foner-type vibrating sample magnetometer at 3.3–67 K and at 78–300 K with a Gouy balance led to an increasing magnetic moment with a maximum of 56.5×10^{-24} J T^{-1}

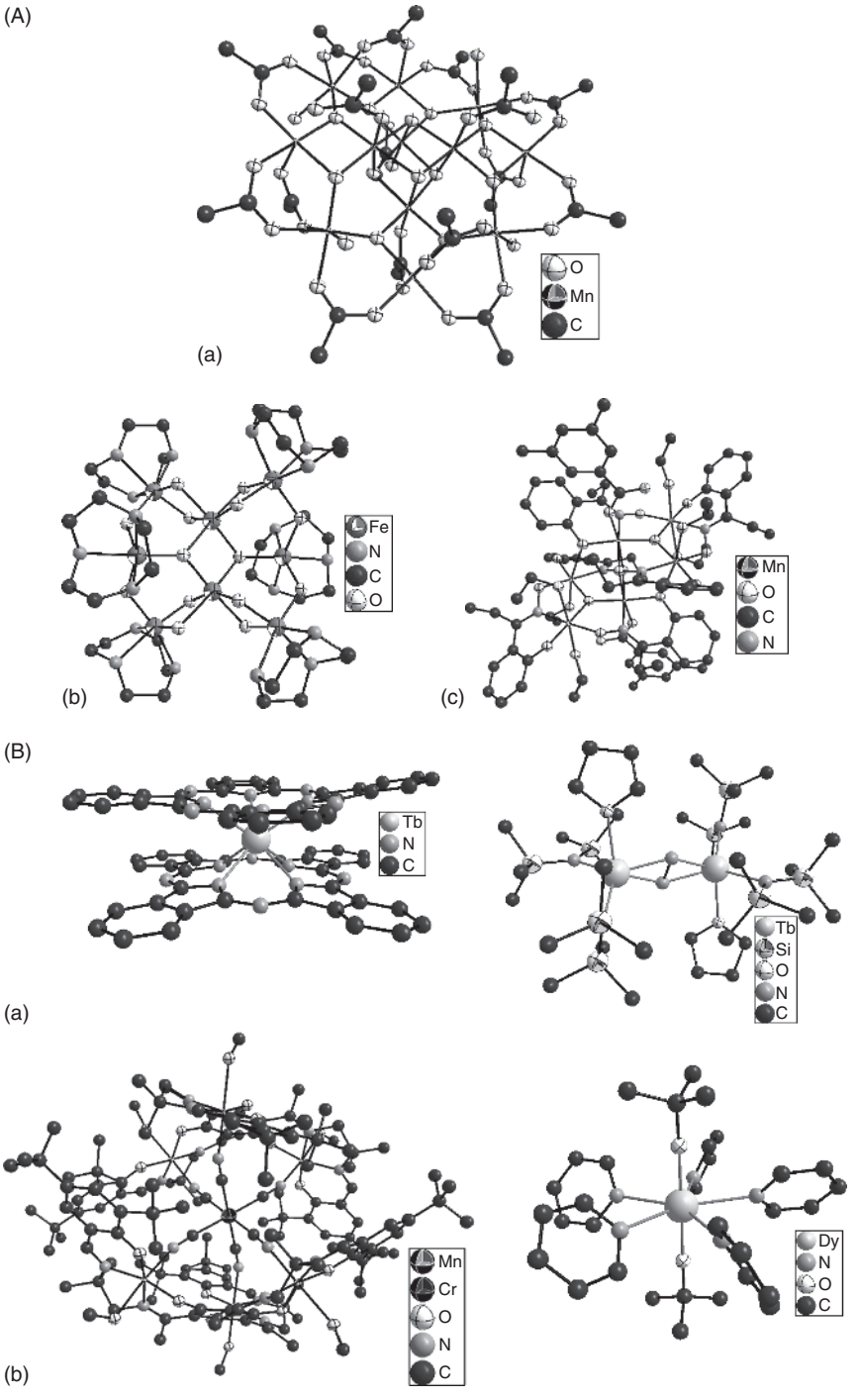

Figure 1.2 (A) Molecular structures of the representative SMMs: SMMs of historical importance (a: $[Mn_{12}]$ [39], b: $[Fe_8]$ [41], c: oxime-bridged $[Mn_6]$ [42], see text). (B) Molecular structures of the representative SMMs: highlights. (a) (left) $TbPc_2$ [43], (right) $[Tb_2N_2]$-core radical-bridged complex [44], (b) (left) rationally designed $[Mn_6Cr]$ [45], (right) record energy barrier complex [Dy] [32] (see text).

at 17–31 K with a sudden drop at lower temperatures. However, it was stated that: "if exchange between all twelve Mn(1), Mn(2) and Mn(3) high-spin atoms is assumed to be via O atoms, such a complicated dodecameric unit should have interesting magnetic properties."

In the early 1990s, Gatteshi and coworkers from the University of Florence revived the story of the $[Mn_{12}]$ complex. Studies of the magnetic properties of the $[Mn_{12}]$ complex led Gatteshi and coworkers to the assumption of a spin ground state at $S = 10$, compatible with all Mn(III) spins up and compatible with all Mn(IV) spins down resembling the behavior of superparamagnets [46]. The magnetic behavior of the $[Mn_{12}]$ complex was explained on the assumption that the magnetization has a purely molecular origin. The pioneering studies of the magnetization relaxation dynamics were performed, which formed the basics of the currently available SMM analyzes. Details of these analyzes will be explained in Chapter 2.

Later studies, especially the extensive work by Christou and coworkers [47–49], led to more insights into the $[Mn_{12}]$ compound in each possible modification addressing not only the structure of the organic ligands but also the oxidation states of the metal ions. Thus, for instance, also t-butylacetate, stearate, or trifluoroacetate analogues were introduced [50–52]. Such ligand substitution reactions could be achieved through the original comproportionation method or a ligand exchange, e.g. in toluene. Sulfur-based side groups were also inserted into the $[Mn_{12}]$ core with a view to facilitate future deposition on gold surface [53–55]. Another possibility was to substitute only some ligands as part of a site-selective substitution, taking advantage of the Jahn–Teller effect for the Mn^{3+} ions. Reaction with iodides led to reduced $[Mn_{12}]$ complexes [48].

The $[Mn_{12}]$ molecule was referred to by Prof. George Christou in his excellent review of a "Drosophila" of SMM science [56]. This is because the most known research species in genetics is the fruit-fly (*Drosophila melanogaster*), which exhibits a role similar to that played by the $[Mn_{12}]$ complex in the field of SMMs.

In studies of relaxation of magnetization, the so-called Jahn–Teller isomerism was found to occur in solid phase, leading to two different ac out-of-phase signals.

Ultimately, the spin ground state of $[Mn_{12}]$ is $S = 10$, and the energy barrier of ~70 K with a blocking temperature of ~3 K. This blocking temperature was a record value for almost 10 years.

In 1996, quantum tunneling of magnetization was experimentally confirmed to occur in $[Mn_{12}]$ by Friedmann et al. [57]. These observations were also reported by Hernandez and coworkers [58] and Thomas et al. [59], warranting new breakthroughs in SMM science. This relaxation mechanism could be found experimentally in the form of characteristic steps on magnetization hysteresis curves.

Another SMM model studied with respect to many aspects was the $\{[(tacn)_6Fe_8(\mu_3\text{-}O)_2(\mu_2\text{-}OH)_{12}]Br_7(H_2O)\}Br{\cdot}8H_2O$ complex (tacn = 1,4,7-triazacyclononane, Figure 1.2Ab) first synthesized by Wieghardt et al. in 1984 [41] and identified as an SMM in 1993 [60]. In this cationic complex, the Fe^{3+} ions are linked by 12 μ_2-hydroxo bridges and by 2 μ_3-oxo bridges. Six terminal tacn ligands cap only six of the eight Fe^{3+} cations. The cation has high charge of +8, which is compensated by bromide counter ions. The cation structure leads to spin frustration, which makes it difficult to predict the spin ground state. The magnetic properties

show ferromagnetic behavior of the χT product and lead to a spin ground state of $S = 10$. This could correspond to six Fe^{3+} spins ($S = 5/2$) up and to two spins down. The magnetic anisotropy of this model compound was carefully studied with EPR. The chemical nature of the complex allows also to employ Mössbauer spectroscopy, which will be covered in detail in Chapter 5. The $[Fe_8]$ complex, in comparison to the $[Mn_{12}]$ compound, shows smaller zero-field splitting (ZFS) but the presence of "steps" on the hysteresis curves of magnetization and QTM has a major impact on its properties as SMM [61]. Detailed account of these properties can be found in the extensive reviews published by Gatteschi and Sessoli [62, 63].

The first metal complex with a blocking temperature of more than 2 K, after the famous $[Mn_{12}]$ compound, was $[Mn^{III}{}_6O_2(sao)_6(O_2CPh)_2(EtOH)_4]$ (sao = doubly deprotonated salicylaldoxime, Figure 1.2Ac) which comprises two triangular $[Mn^{III}{}_3O]$ units with a central μ_3-oxo ligand and bridging oxime groups at the edges of the formed triangles [64]. These units are linked through two Mn—O bonds. The oxime groups are donated by six salicylaldoxime ligands, there are also two terminal benzoate ligands in the complex molecule. For this complex the ac out-of-phase signals at 1–1000 Hz were detected at 1.96–3.30 K. The effective energy barrier to spin reversal was found at 28.0 K with $\tau_0 = 3.6 \cdot 10^{-8}$ s and spin ground state of $S = 4$. This promising initial platform was improvised later on by manipulating the bulk bridging ligand [42]. Replacement of the salicylaldoxime with ethyl-substituted salicylaldoxime ligand and the terminal benzoate with a 3,5-dimethylbenzoate ligand resulted in a further distortion of the $[Mn^{III}{}_6O_2]$ core. Thus the spin ground state of $S = 12$ was achieved with a record-breaking blocking temperature of 4.5 K and the effective energy barrier to spin reversal at 86 K.

Systematic studies of a series of complexes with a substituted salicylaldoxime ligand allowed to correlate the Mn–N–O–Mn torsion angle of the central $[Mn^{III}{}_6O_2]$ unit with the dominant magnetic coupling of the Mn^{3+} ions [42]. A "magical" value of ~31° was found above which the dominant coupling was ferromagnetic with a high spin ground state up to 12.

Further research explored the rich chemistry of different oxime ligands leading to new topologies of homo- and heterometallic compounds. The chemical aspects of SMM science published during recent years will be described in Chapter 6.

Further insights into the features of SMM behavior allowed to derive other guidelines for the design of SMMs. For instance, the importance of a high-spin ground state was undermined by publication of an $[Mn_{19}]$ complex with a mixed-valence $[Mn^{III}{}_{12}Mn^{II}{}_7]$ core and a record spin ground state of 83/2 which did not display SMM behavior, obviously due to too low magnetic anisotropy [65].

On the other hand, in 2003, Ishikawa reported on the first mononuclear SMM, $[Tb(pc)_2]^{n-}$ (Figure 1.2Ba) with a huge leap in the energy barrier, this time reaching the value of 790 K [11]. With this discovery, a new type of SMMs was introduced, based on orbital and spin angular moments of a single lanthanide ion, governed by the ligand field. The first indicates that this discovery could possibly stem from Ishikawa's study on multidimensional minimization analysis of the magnetic susceptibility and ^{1}H-NMR data [66]. A comprehensive study of a series of

$[Pc_2Ln^-]\cdot TBA^+$ salts (pc = dianion of phthalocyanine, $TBA^+ = N(C_4H_9)_4^+$, Ln = Tb, Dy, Ho, Er, Tm, Yb) showed that only the Tb and Dy are representative of SMMs with slow relaxation of magnetization.

Owing to ease of tracking with scanning tunneling microscopy and manipulation, the $[Tb(pc)_2]^-$ was subject to many pioneering studies targeting at applications in spintronics. The recent progress is briefly reviewed in Section 1.3.5.

This complex was also subject to further improvements. For instance, de la Torres and coworkers managed to increase the effective energy barrier to spin reversal to 938 K by modifying one of the phthalocyanine ligands via peripheral substitution to achieve a heteroleptic [Tb(pc)(pc′)] complex [67].

Following the success with strong magnetic anisotropy of the lanthanide complexes, a logical research target in SMM science was the complexes formed by actinides. Despite the limited range of applications due to radioactivity issues they still represent an interesting subject for research bringing new insights into the fundamentals of SMM behavior. The first report on the actinide-based SMM was with regard to a uranium(III) complex [68].

Recently, Long and coworkers [69] showed that mononuclear SMMs can be formed not only by 4f/5f metals but also by 3d metals. Several features of these metals hamper the detection of an SMM property. The spin–orbit coupling in the first-row 3d metals is lower and the orbital moment is usually quenched by the ligand field. Molecular vibrations affect the degeneracy of the d orbitals and lead to a weaker ZFS. The first 3d-metal-based SMM was a high-spin Fe(II) complex ($[(tpa^{mes})Fe]^-$ where tpa^{mes} = mesityl-substituted tris(2-pyridylmethyl)amine) [69]. The complex displays an $S = 2$ spin ground state, an effective energy barrier to spin reversal at 60.4 K. Owing to slight deviation from a threefold symmetry a transverse component of the magnetic anisotropy is also observed, leading to additional tunneling pathways that decrease the theoretically achievable energy barrier of 227.3 cm^{-1}. Circumventing this challenge was listed as one of the future research directions.

A two-coordinate low-valent iron(I) compound was also shown by Long and coworkers [70] to display SMM behavior. This was achieved by a good understanding and modeling of the crystal field effects. The central ion adopts a low oxidation state, ensuring a high-spin d electron configuration and d electrons located in close-lying d orbitals. The linear geometry of the complex favors the formation of an easy axis of magnetization. A high effective energy barrier to spin reversal at 328 K was reported.

A considerable rise in the blocking temperatures was achieved in the radical-bridged 4f complexes by the same group that introduced the first 3d-metal-based SMMs. In 2011, Long and coworkers reported a series of dinuclear N_2^{3-}-bridged complexes, $[K(18c6)(THF)_2]\{[(Me_3Si)_2N]_2(THF)Ln\}_2$ [13]. These products were obtained in a reaction of the $\{[(Me_3Si)_2N]_2(THF)Ln\}_2$ complex with potassium graphite and 18-crown-6 in tetrahydrofurane (THF). The applied strategy was to overcome the usually observed weakness of Ln···Ln interactions involving f orbitals by the use of radical bridging ligands. For the Dy(III) complex, a record blocking temperature of 8.3 K was reported at a sweep rate of 0.08 T s^{-1}. The Gd(III) analogue turned out to display the strongest magnetic

coupling. The driving force behind these remarkable features was proven to be the intramolecular exchange coupling.

In a later report from the same group, further progress was achieved by introducing a radical-bridged terbium complex exhibiting magnetic hysteresis at 14 K [44]. The same reduction of N_2-bridged lanthanide complexes by potassium graphite yielded new Tb, Ho, and Er analogues. The new record-breaking Tb complex displayed also multiple relaxation processes. Thus, the Long group doubled and quadrupled the record for the blocking temperature in SMMs within a short time-span. In Chapter 7 the radical-bridged SMMs will be reviewed in detail.

The field of SMM science is still rapidly developing as evidenced in the next sections on their recent progress.

1.3 Recent Progress

The past years have brought much progress into the field of SMM science and many new unexpected directions emerged.

The field is highly interdisciplinary as SMMs may find different applications. Their sophisticated structures and chemistry are interesting for a chemist, their quantum phenomena are fascinating for a physicist, and they may serve as drug carriers in medicine, to name only a few. Perhaps, the most frequently mentioned is in terms of increasing the data storage density. As predicted by Moore's law, the miniaturization of electronic data carriers is expected to progress and physical limits may stop us from utilizing this technology. On the other hand, applying a "bottom-up" approach, magnetic molecules could be organized on the memory carriers and much more data than has been achievable so far could be input. In the following sections some recent achievements will be highlighted. The presented overview is not exhaustive and should be regarded as an appetizer – many topics will be covered in more detail in the following chapters.

1.3.1 SMMs Based on Actinides

The progress in actinides-based SMMs started with the introduction of the first uranium(III)-based representatives ($U(Ph_2BPz_2)_3$) [68–72] and has resulted in some new developments in recent years. Much of the new facts in actinides chemistry were discovered by Liddle et al. Meihaus and Long provided in 2015 an excellent tutorial review on fundamental aspects of the actinide-based SMMs [72]. In the actinide ions the spin–orbit coupling is stronger than the crystal field splitting. The source of the magnetic anisotropy is crystal field splitting, giving rise to M_J-microstates. Future developments should aim at addressing the understanding of the electronic structure and magnetism as well as its dynamics in 5f compounds [71].

Most of the known actinide-based SMMs are uranium(III) complexes. U^{3+} ($5f^3$) is a Kramers ion, displaying a large total angular momentum ground state, $J = 9/2$, with oblate-type anisotropy. A good overview of recently discovered actinide-based SMMs is provided by Meihaus and Long [72].

In the first known uranium(III) SMM, mononuclear $U(Ph_2BPz_2)_3$, thermally activated slow magnetic relaxation was observed under zero applied field with the effective barrier to spin reversal of 28.8 K and the relaxation time $\tau_0 = 10^{-7}$ s [71]. In later studies, this complex molecule was modified, e.g. by removing the phenyl groups from the organic ligand to obtain $U(H_2BPz_2)_3$ with axially elongated coordination polyhedron, as compared to $U(Ph_2BPz_2)_3$ [73]. For the field values higher than 500 Oe an additional relaxation process was observed, most probably as a consequence of intermolecular interactions. Further studies on uranium(III) scorpionate complexes revealed that for the isostructural $U(Bc^{Me})_3$ ($[Bc^{Me}]^-$ = dihydrobis(methylimidazolyl)borate anion) and $U(Bp^{Me})_3$ ($[Bp^{Me}]^-$ = dihydrobis(methylpyrazolyl)borate anion) compounds, the donor power of the *N*-heterocyclic carbene ligands helps to influence the temperature dependence of the slow relaxation of magnetization [74]. For the $U(Bc^{Me})_3$ compound, a moderate effective energy barrier to spin reversal of 33.1 K was found. Similar values were found for other uranium(III) scorpionate complexes, including $[UTp^{Me2}{}_2(bipy)]I$ ($[Tp^{Me2}]^-$ = hydrotris(dimethylpyrazolyl)borate anion, bipy = 2,2′-bipyridine) and $[UTp^{Me2}{}_2]I$ with energy barriers at 26.2 and 30.2 K, respectively [75]. Other recently reported mononuclear uranium(III) SMMs include $[U(Tp^{Me2})_2(bipy)]^+$ cationic complex ($[Tp^{Me2}]^-$ = hydrotris(dimethylpyrazolyl)borate anion, bipy = 2,2′-bipyridine) with an energy barrier at 26.2 K. An organometallic dinuclear uranium(III) complex, $[U(BIPM^{TMS}H)(I)]_2(\mu\text{-}C_6H_5CH_3)$ ($BIPM^{TMS} = C[PPh_2NSiMe_3]_2$), was found to show slow relaxation of magnetization under a dc field of 0.1 T; however, no relaxation times could be extracted from the available data [76]. Studies of a series of structurally unrelated trivalent uranium complexes emphasized the low dependence of this ion on the symmetry of the surroundings or ligands [77].

SMM behavior was also reported for uranium complexes at oxidation states other than +3. The uranium(V) UO(TrenTIPS) (TrenTIPS = $[N(CH_2CH_2NSi^iPr_3)_3]^{3-}$) complex displays a slow relaxation of magnetization only when an applied dc field is present, with an effective energy barrier to spin reversal at 21.4 K and magnetic hysteresis loops up to 2.4 K [78]. Despite the unfavorable electron configuration of uranium(IV) (f^2 system, $^3H_4$ ground state, orbital singlet ground state at low temperatures, non-Kramers ion) there also exist examples of the first uranium(IV)-based SMM: $[\{(SiMe_2NPh)_3\text{-tacn}\}U^{IV}(\eta^2\text{-}N_2Ph_2{}^{\cdot})]$ [79]. The compound was synthesized as a result of a one-electron reduction of uranium(III) starting mononuclear complex with azobenzene. In fact the starting uranium(III) substrate, $[U^{III}\{(SiMe_2NPh)_3tacn\}]$, was also the first uranium(III) complex that exhibited slow relaxation of magnetization at low temperatures, from 1.7 K. Observation of SMM behavior in the uranium(IV) product was possible due to the employment of a radical ligand, assisting the slowing down of quantum tunneling of the magnetization. Obviously, this ligand switches U^{4+} to a Kramers ion.

The transuranic SMMs are extremely rare and only a handful of recent examples are known. An inherent problem affecting the studies of magnetic properties at low temperatures are self-heating effects due to radioactive decay. The Mössbauer spectra recorded at 4.2 K for a homoleptic $Np^{IV}(COT)_2$ (COT = cyclooctatetraenyl) complex of D_{8h} molecular symmetry already pointed

to the phenomenon of slow spin–lattice relaxation [80]. The complex shows slow relaxation of magnetization under applied dc fields of more than 0.1 T. Despite the previous observation of slow magnetic relaxation and superexchange interaction in other trimetallic Np complex [81], the $Np^{IV}(COT)_2$ complex is the first example where also butterfly-shaped magnetic hysteresis curves and the resulting magnetic memory effects were detected. Ac magnetic susceptibility studies led to the assumption of different relaxation mechanisms. It was shown that in spite of a relatively low-spin ground state no saturation is achieved even at 14 T. All these effects allowed the authors to expect that 5f-based SMMs should display higher energy barriers to spin reversal and larger coercive fields than their 4f-based analogues. However, in contrast to the 4f systems, the current experimental values for energy barriers in actinide-based SMMs are much lower than their theoretical predictions. Several reasons for this were listed in the review of Meihaus and Long [72], including the view that the ground M_J state is not maximal for the mononuclear complexes. A remedy for this could include manipulation of the coordination sphere symmetry and the metal–ligand distances, which would be a significant synthetic challenge.

With the advent of organometallic SMMs, described more in detail in Section 1.3.2, new elements and oxidation states turned out to be accessible for f-electron-based SMM science. Dutkiewicz et al. [82] synthesized a transuranic neptunium(III)-based organometallic SMM, providing also more insights into the covalent part in the metal–ligand bonding. The complex, formed in a reaction of $^{237}NpCl_4$ with K_2L^{Ar} (H_2L^{Ar} = *trans*-calix[2]benzene[2]pyrrole), is [$(L^{Ar})^{237}$NpCl]. Most probably the slow relaxation of magnetization takes place under the experimentally inaccessible temperature range of below 2 K, as evidenced by the ac studies results with an increase in ac susceptibility below 10 K.

In 2014, Magnani, Caciuffo et al. reported on the first plutonium-based SMM, [tris(tri-1-pyrazolylborato)plutonium(III)] of C_{3h} molecular symmetry [83]. The SMM behavior was identified based on slow relaxation of magnetization detected at temperatures below 5 K. The effective energy barrier was found to exceed five times this value for the isostructural uranium(III) analogue. However, the hysteresis loops of magnetization were not observed down to 1.8 K.

Owing to the rich chemical properties of plutonium, with five different oxidation states, more interesting information on the chemistry of SMMs and the opportunities to conduct systematic studies can be expected in the future. As there are more analogous actinide SMMs with the same ligand, the homoscorpionate complexes can be considered as model compounds.

Polynuclear actinide complexes have also been investigated [76, 81, 84–88]. Particularly promising is the perspective of using radical bridging ligands, which helped to enhance the magnetic properties of lanthanide-based compounds dramatically [13]. As compared to lanthanides, the actinides show higher spin–orbit coupling effects, and the 5f orbitals, as compared to the 4f orbitals, show higher radial distribution and, as a consequence, the covalency of the bonds involving these orbitals may be higher, leading to stronger magnetic coupling [72]. Nevertheless, the actinide-based systems are still challenging in terms of rational

design, predominantly due to the bonding covalency issues, oxophilic properties, and large radii range of actinides, as compared to lanthanides [72].

Strong magnetic coupling in polynuclear actinide complexes, suppressing quantum tunneling of magnetization, was mentioned as a key factor in the development of actinides-based SMM science by Liddle and van Slageren [89]. Particularly attractive are the uranium(V) complexes, also in combination with 3d metals [90, 91].

The first polynuclear actinide-based SMM was the triangular mixed-valence complex $(Np^{VI}O_2Cl_2)[Np^{V}O_2Cl(THF)_3]_2$ with two chloride-bridged neptunyl(V) moieties, capped with a neptunyl(VI) group [81]. In this complex, strong coupling of Np^{5+} and Np^{6+} ions was observed. The slow relaxation of magnetization was detected already under no applied dc field. The effective energy barrier to spin reversal of 140 K is higher than the values achieved in mononuclear actinide complexes. One of the possible interpretations of the magnetic behavior of this compound was the excited $M_J = \pm 5/2$ state of Np^{6+} and a single-ion origin of the SMM property.

A mixed 3d–5f complex comprising uranyl(V) moieties and Mn^{2+} ions was introduced by Mazzanti and coworkers [84], motivated not only by its expected interesting magnetic properties but also because of its relevance to environmental clean-up strategies. This compound is a wheel-like $\{[UO_2(salen)]_2Mn(py)_3\}_6$ (py = pyridine) complex obtained by the reaction of $[Cp^*_2Co][UO_2(salen)(py)]$ ($[Cp^*]^-$ = decamethylcyclopentadiene anion) with $Mn(NO_3)_2$. Interestingly, when $CaCl_2$(DME) (DME = dimethoxyethane) substrate was used instead of $Mn(NO_3)_2$, only a lower-nuclearity complex $\{[UO_2(salen)_4]Ca_2\}$ could be isolated. The UO_2–Mn complex shows an open magnetic hysteresis loop at low temperature, non-zero coercive field below 4 K and evidence of quantum tunneling steps below 2.5 K. In this case, SMM behavior was detected for the first time in a 3d–5f assembly, in spite of the previous studies in which evidence of a magnetic exchange in such a heterometallic trinuclear/dinuclear complexes [92–95] was found. Thus, control of a 3d–5f cation–cation interaction turned out to be a good strategy to construct heterometallic SMMs.

1.3.2 Organometallic SMMs

Initially, SMM research was focused on coordination compounds, a good representative being the "archetypic" $[Mn_{12}]$ complex. In spite of the advanced stage of development and well-controlled principles in the synthesis of organometallic compounds, these were scarcely used in SMM science until recently. The organometallic approach has been popularized in particular by Layfield and reviewed in 2014 [96]. The first report on an organometallic SMM appeared in 2010. These are $[\{Cp_2Dy(\mu\text{-bta})\}_2]$ (**1**) (btaH = 1*H*-1, 2,3-benzotriazole) and $[\{Cp_2Dy[\mu\text{-N(H)pmMe}_2]\}_2]$ (**2**) (NH_2pmMe_2 = 2-amino-4,6-dimethylpyrimidine) compounds showing similar behavior of their magnetic properties. However, weak interaction between the Dy^{3+} ions in **2** clearly hampers the observation of SMM properties in this case. Thus only **1**, with

electronically isolated Dy^{3+} ions, is an SMM with the effective energy barrier to spin reversal of ca. 57 K. The currently known organometallic SMMs include mainly 4f and 5f systems, but 3d systems have also been reported. Some of these SMMs have already been mentioned in the previous sections.

Harriman and Murugesu [97] have recently demonstrated an organolanthanide building block approach to SMMs. The strategy was to use highly anisotropic late 4f elements, Dy^{III} and Er^{III}, as metallocenes with COT and the related ligands, in spite of their sensitivity to air and moisture. In this approach, the organic ligand π-electron clouds are used to assist Ln···Ln interactions by perturbing their shielded 4f orbitals. Sandwich-like molecular architectures are targeted, reminiscent of the success of Ishikawa's $Tb(Pc)_2$ molecule, being a sandwich-type complex of phthalocyanine. Successful output includes an Er^{III} derivative $[Er^{III}{}_2(COT'')_3]$ (COT″ = 1,4-bis(trimethylsilyl)cyclooctatetraenyl dianion), reaching blocking temperature of 14 K in frozen solution and magnetic hysteresis up to 12 K in solid state. Exchange interaction between the Er^{3+} ions was listed as the reason for enhancement of the SMM properties as compared to the mononuclear precursor used to synthesize this remarkable compound. It was shown on the example of some model compounds how critical the impact of molecular symmetry is on the overall SMM properties. Synthetic challenges of controlled stacking of multiple sandwich-type complexes need to be addressed in the future. In particular, the prospect of creating chains of the successful building units seems to be very intriguing.

Clérac, Smith, and coworkers [98] showed how exploring new synthetic routes can lead to new organometallic SMMs. An incomplete nitrogen atom transfer from the $PhB(MesIm)_3Fe^{IV}N$ (where $[PhB(MesIm)_3]^-$ = phenyltris(1-mesitylimidazol-2-ylidene)borate) to the $V^{III}(Mes)_3(THF)$ complex led to a bimetallic $PhB(MesIm)_3Fe\text{-}N{=}V(Mes)_3$ product. In this product the high-spin Fe^{II} and V^{V} centers are linked through a linear nitride bridge. The two-electron transfer occurrence is confirmed spectroscopically. The product is an SMM with slow relaxation of magnetization under applied dc field and an effective energy barrier to spin reversal of ca. 10 K. The source of the SMM behavior is the high-spin Fe^{2+} ion. It is expected that application of the discovered synthetic principle to other low-coordinate complexes will yield products with even more magnetic centers linked by nitride bridges.

Layfield and coworkers [99–101] introduced a series of SMMs containing a dysprosium metallocene unit $\{Cp'_2Dy\}$ (Cp′ = substituted cyclopentadienyl) with soft donors as bridging ligands: $[Cp'_2Dy(\mu\text{-}X)]_n$ (n = 2, 3, e.g. X = P, As, S, Se). As a continuation of this research, Layfield and coworkers [102] recently reported on a new low-symmetry dysprosium metallocene SMM with a high anisotropy barrier. The compound is an isocarbonyl-ligated $[Cp^*_2Dy\{\mu\text{-}(OC)_2FeCp\}]_2$ complex with a rhombus-shaped $[Dy_2Fe_2]$ core. The complex was obtained in the salt elimination reaction of $[Cp^*_2M(\mu\text{-}Ph)_2BPh_2]$ (M = Y, Dy; Cp* = pentamethylcyclopentadienyl) with K[Fp] (Fp = $CpFe(CO)_2$), along with its yttrium-analogue used for the sake of comparison. As a result of a strong axial ligand field of the cyclopentadienyl ligands a large energy barrier to spin reversal of 662 cm^{-1} under zero applied field is observed. The computational

studies revealed an unprecedented pathway of the magnetization in this case, through at least the fourth-excited Kramers doublet, and probably also through the fifth- and sixth-excited states which is seen as a good guideline for the future design of organometallic SMMs.

1.3.3 Rational Design of SMMs

Owing to many often serendipitous syntheses reported for SMMs a need was identified to rationalize their design [103]. First ideas of such a rationalization came up with investigation on the potential barrier U_{eff}. It is defined as $U_{eff} = |D|\ S^2$ for integer spins and $U_{eff} = |D|\ (S-0.5)^2$ for half-integer spins with D = zero-field splitting and S = spin ground state. Control of D is hard to accomplish but can be directed through choice of metal and, therefore, highly magnetically anisotropic metals, such as Mn(III) or lanthanides, are favorable. Also, it is evident that a high-spin ground state increases the potential barrier [104–108].

This could be achieved by the use of linking functional groups, such as oximes or carboxylic acids, along with metal ions with high-spin state like (d^4–d^6). Such first design criteria led to advances in the field, concentrating on the high-nuclearity clusters with manganese. The previously mentioned "magic" angle for oximes was an alternative which also led to further improvements. This culminated in the synthesis of an [Mn_{84}] cluster, but its magnetic properties were far behind expectations [109] and other high spin record holder, such as the [Mn_{17}] complex with $S = 37$, did not display enhancements in their SMM properties [110, 111]. Altogether it was concluded that the ZFS parameter D and the spin ground state S should not be optimized independently [112–114].

This opened the scope to ligands that tend to propagate ferromagnetic coupling and to the use of magnetically anisotropic ions rather than to maximize the cluster size. As the understanding of the processes progressed, quantum tunneling of magnetization was considered a serious problem [57, 59, 115, 116]. It was shown that it strongly depends on the symmetry of the complex and vanishes for at least trigonal symmetry through minimization of the rhombic components in the magnetic anisotropy. This criterion had a major influence on the field and ligands were developed to direct C_3 symmetry on the cluster. Glaser [117] focused on a phloroglucin backbone with three salene units attached to it. This ligand also included the possibility to propagate ferromagnetic coupling through a spin polarization mechanism which could be perfectly achieved in a phloroglucin-backbone. The use of this ligand yielded bowl-shaped trinuclear clusters with favorable ferromagnetic coupling. In a further step, a reaction of the compound was performed with hexacyanidometallates to maximize the spin ground state and add even more anisotropy to the system.

Thus, for instance, a series of isostructural cationic complexes $[Mn^{III}{}_6M]^{3+}$ ($M = Cr^{III}$, Fe^{III}, Co^{III}) could be isolated, among which the Cr(III) product is an SMM (Figure 1.2B) [117]. Based on this example, general trends possibly leading to optimization of the SMM property were analyzed. The role of attractive van der Waals interactions between two bowl-like units capping the central

hexacyanidometallate moiety was underlined and showed to influence the magnetic coupling. In order to increase the energy barrier, such steric factors would need to be considered without biasing the ability of the used building blocks to self-assembly. Other important factors are solvent coordinating to the metal ions, intermolecular interactions in the crystal structure, and stabilization of the spin ground state via increase in the contribution of the spin-delocalization mechanism. The last factor could be manipulated through exchange of hydroxyl O atoms in the phloroglucyl backbone with softer sulfur atoms. The whole arsenal of organic chemistry of the ligand could also be employed to influence its aromaticity, e.g. by exchanging the imine units with amine groups [117].

Christou and coworkers [118] developed a magnetostructural correlation useful for studies of molecular magnetism, predicting the exchange interaction constant between two Fe^{3+} ions, dependent on the Fe—O bond lengths and Fe–O–Fe angles involving the bridging ligands. In this study, polynuclear Fe(III) complexes of 8-hydroxyquinoline (hqnH), $[Fe_8O_4(O_2CPh)_{10}(hqn)_4(OMe)_2]$, and $[Fe_6O_2(OH)_2(O_2CPh)_{10}(hqn)_2]$, were investigated. The developed correlation was successfully used to interpret the magnetic properties of the lower-nuclearity Fe complexes reported in literature.

Systematic computational studies also provide insights and conclusions that could be useful for rational design of SMMs. Aravena et al. [119] studied with ab initio calculations and ligand field analysis three $[M(\gamma\text{-}SiW_{10}O_{36})_2]$ ($M = Mn^{III}$, Fe^{III}, Co^{II}) complexes previously obtained by Sato et al. [120]. These model compounds were the first rigid polyoxometalate (POM)-based SMMs with single transition metal ions, showing SMM behavior under the applied dc field. For the Co(II) and Mn(III) complexes, the magnetic properties could be rationalized in terms of low-energy excitations, of higher energy for Mn(III). This results in a strong unquenched ground-state momentum for the Co(II) complex and no measurable energy barrier for the Mn(III) complex. For the Fe(III) complex, the presence of low-lying quartet and doublet Fe(III) states was used to explain the small relaxation barrier for normally magnetically isotropic high-spin d^5 electron configuration. In this case the rigid POM ligand imposes an axially elongated coordination environment on the central Fe^{3+} ion. It was possible to reproduce the ZFS parameter significantly for the Co(II) case but for Mn(III)/Fe(III) the values were underestimated due to the possibility of specific-multiplicity states transitions that were absent for Co(II).

Another step toward rational SMMs, in particular for applications in data storage, was reported by Cador and coworkers [121]. A model $[Dy(tta)_3(L)] \cdot C_6H_{14}$ ($tta^- = 2$-thenoyltrifluoroacetonate and L = 4,5-bis(propylthio)-tetrathiafulvalene-2-(2-pyridyl)-benzimidazole methyl-2-pyridine) solid complex displaying SMM behavior was subject to isotopic enrichment experiments. In the initial product four stable abundant isotopes were present, ^{161}Dy (18.9%) and ^{163}Dy (24.9%) with $I = 5/2$, as well as either the ^{161}Dy or ^{164}Dy (28.2%) isotopes without non-zero nuclear spin. This product was enriched with either the ^{161}Dy or ^{164}Dy isotope. Such isotopic enhancement had a drastic effect on the thermally independent relaxation of magnetization: for the "magnetic" ^{161}Dy isotope relaxation time increased 10 times. Thus the data storage capability could be improved in a targeted way with this approach.

1.3.4 Quantum Computing

Owing to their magnetic bistability and demonstration of quantum phenomena, SMMs are promising candidates for applications in quantum computing.

Quantum computing has already reached the stage of commercialization. Quantum computers use atoms and molecules to perform memory and processing tasks. Initially, theoretical considerations on quantum computers were proposed in 1982 by Benioff [122]. Quantum computing makes use of phenomena such as superposition and entanglement of states. This could revolutionize areas such as encryption or quantum simulation. A prototype theoretical model of a quantum computer is the so-called "quantum Turing machine." The equivalents of traditional bits are the so-called qubits which may adopt also a superposition of "0" and "1" states. Application of SMMs as qubits is limited by their spin–lattice relaxation times that should be long enough to afford long spin–spin relaxation time but short enough for an optimal qubit reset time [123]. Qubits could also be realized as photons, ions trapped in potential wells or superconducting circuits [124].

The first quantum computing company was founded in 1999 in Vancouver (Canada). The goal of this company is development, fabrication, and integration of superconducting quantum computers. In 2010, the first commercial system, the D-Wave One quantum computer, was released. In 2013, a 512-qubit D-Wave Two system and in 2015 a 1000+ qubit D-Wave 2X system was announced. The latter system can evaluate 2^{1000} possible solutions at the same time, using a quantum annealing algorithm. So far, the D-Wave systems have been used, e.g. in the aerospace industry (Lockheed Martin, NASA).

Using the example of a [Dy-radical]· · ·[radical-Dy] SMM, Clérac, Preuss, and coworkers [125] showed how its dynamics can be fine-tuned by the exchange-bias and an applied magnetic field. The considered model complexes are mononuclear, forming a dimeric unit through weak intermolecular interactions. The constituent Dy^{3+} ions are not related by any crystallographic symmetry element. The applied ligand is radical – 4-(benzoxazol-2-yl)-1,2,3,5-dithiadiazolyl (boaDTDA) which in reaction with $Dy(hfac)_3(DME)$ (DME = 1,2-dimethoxyethane) forms an eight-coordinate complex $Dy(hfac)_3(boaDTDA)$. The authors show that the complex is an SMM with a single set of thermal and quantum relaxation modes and acts as a single supramolecular entity. It is possible to "decouple" the weakly interacting Dy^{3+} ions with a weak dc field. Moreover, the interpretation of these results is supported by studies of the Gd and Y analogues.

Pedersen, Piligkos and coworkers [123] detected quantum coherence in an SMM Yb(trensal) (H_3trensal = 2,2′,2″-tris(salicylideneimino)triethylamine)). The compound is modifiable with organic substituents, photoluminescent and sublimable. Moreover, it displays a very large gap between the electronic ground doublet and the first excited ligand field state, displaying a slow paramagnetic relaxation effect at the same time. The complex is incorporated in an isostructural crystal of diamagnetic Lu(trensal). Future studies will aim at further extension of the spin–lattice relaxation times.

One of the few examples of potential molecular qubits showing room-temperature quantum coherence was reported by Sessoli and coworkers [126]. The

corresponding system is VOPc SMM dispersed in an isostructural TiOPc matrix. The system was extensively studied employing pulsed EPR spectroscopy and ac susceptibility measurements. Quantum coherence with $T_m \sim 1\,\mu s$ was detected at 300 K, being the highest value obtained so far for molecular electronic spin qubits.

On the other hand, alternative approaches are also available and Freedman and coworkers [127] reported on a nuclear spin-free chromium complex for which forbidden transitions could be employed as qubits. This study is an experimental demonstration of the model previously proposed by Leuenberger and Loss for high-spin molecules [128].

One of the most fascinating prospective applications of SMMs is in data storage. As the famous Moore's law states, the number of transistors on a microprocessor doubles every 18 months, which drives the need for device miniaturization.

The data storage densities reached up to 345 Gbits in.$^{-2}$ with a growth of 100% in 2009. The use of SMMs could improve this number by a factor of 10^4 [129]. SMMs could be considered as qubits, being the processing elements of quantum computers. These computers could make use of such quantum phenomena as entanglement/superposition of states. A system of two weakly interacting SMMs could serve as a model for a 2-qubit quantum gate [130].

Salman and coworkers [131] used muon relaxation and ac susceptibility measurements to investigate the magnetic properties of the $[Dy(hfac)_3(PyNO)]_2$ (PyNO = pyridine-*N*-oxide) SMM deposited on polycrystalline-gold-coated mica surface via a sublimation–resublimation process. The compound was proved to retain its chemical integrity and SMM behavior. This is observed in spite of the significant differences of the packing of the SMM molecules in crystalline phase as compared to their distribution on the investigated substrate. Molecular spin fluctuations were studied in detail and shown to display no depth dependence of the spin correlation time, contrary to other studied SMMs, such as $TbPc_2$.

Suitable choice of the deposition surface may also even enhance the SMM properties, as recently reported by Dreiser and coworkers [132]. The robust $TbPc_2$ SMM was deposited on insulating MgO thin film on Ag(100) to demonstrate unprecedented enhancement of the magnetic remanence and the hysteresis opening. This is observed taking pure Ag(100) surface as a reference for which the magnetic hysteresis opening is barely visible for the $TbPc_2$ molecules. The MgO layer plays the role of a tunnel barrier; it suppresses the strong scattering of conduction electrons from the metal at the molecule and displays weak molecule-surface hybridization. Thus, a combination of SMMs and MgO-based tunnel junctions may lead to SMM-containing tunnel devices in the future.

1.3.5 SMMs in Molecular Machines

Molecular nanomagnets are also potential elements of molecular machines. With further development of microscopic and molecular manipulation techniques it became possible to explore this idea. A particularly successful direction turned out to be the combination of SMMs with carbon nanostructures which yielded

recently many promising results for the use of carbon nanotubes (CNTs) and graphene. Such aggregates could find application in spintronics which is a field combining molecular electronics and spin manipulation. Phenomena observed in SMMs and useful for electron transport in molecular machines include the Kondo effect, quantum tunneling, Berry-phase blockade, spin relaxation, or magnetic switching [133].

van Slageren, Khlobystov, and coworkers [134] successfully encapsulated [Mn_{12}] SMMs in CNTs. The motivation for this study was the possibility to address SMMs in molecular machines without compromising their magnetic properties. CNTs could also protect SMMs from decoherence which is crucial in quantum computing. van Slageren, Khlobystov, and coworkers used wide CNTs with the internal diameter range of 5–50 nm to avoid previously reported problems with adsorption of SMMs, rather than insertion, when thinner CNTs were used. CNTs were pretreated with concentrated nitric acid and heated in air for opening. Supercritical CO_2 was used to transport the [Mn_{12}] molecules inside of the CNTs. An excess of the [Mn_{12}] complex was eliminated by subsequently washing with acetonitrile. The successful insertion and solely weak van der Waals interactions could be confirmed with transmission electron microscope (TEM) images and energy-dispersive X-ray spectroscopy (EDX) analyzes. Extensive investigation of the magnetic properties of this hybrid material led to the conclusion that the SMM properties are fully retained and Jahn–Teller isomerism is detected, as for the bulk [Mn_{12}] sample. The electrical properties of CNTs were found to be modified by magnetoresistance of the [Mn_{12}] complex. The SMM molecules are still mobile inside of CNTs and tend to get aligned with the external magnetic field. The authors predict that this study will be relevant for spintronics, e.g. via precise control of the CNTs electrical conductivity by the magnetic states of SMMs as a method for nanoscale generation of spin-polarized currents. Such materials could become part of ultrasensitive magnetic devices, including a nano-SQUID or a magnetic force microscopy (MFM) probe.

Yamashita and coworkers [135] used a capillary method to encapsulate Dy acetylacetonato SMMs in multiwalled carbon nanotubes (MCNTs). This encapsulation could be followed with transmission electron microscopy and it was shown with ac susceptibility measurements that the encapsulated molecules still behave as SMMs, also inside the nanotubes. The MCNTs were purified and "opened" with usual methods, combined with solution of $Dy(acac)_3(H_2O)_2$ in 1,2-dichloroethane, and treated with heat/ultrasonication. This solution was left uninterrupted for three days to allow for a capillary insertion. The frequency-dependent ac out-of-phase signal was generated for the obtained hybrid material, but no enhancement of the SMM property was observed. Nevertheless, this was the first report on a lanthanoid SMM encapsulated in MCNTs and spintronic devices combining the magnetic/electronic properties of SMM/MCNT hybrids could be anticipated.

Nanotubes could also be constructed from SMMs, which display SMM properties themselves. Powell, Tang, and coworkers [136] reported on hexagonal tubes out of large 3d–4f-based heterometallic macrocycles with inner diameters of 16.4, 16.5, and 16.4 Å, respectively. This arrangement could be confirmed with X-ray diffraction studies. The used macrocycles were [$Dy_6Cu_6(H_2L')_6$

$Cl_{12}(H_2O)_6] \cdot 5ClO_4 \cdot OH \cdot 30H_2O$, $[Dy_6Cu_6(H_2L')_6Br_{12}(H_2O)_6] \cdot 5ClO_4 \cdot OH \cdot 6H_2O$, and $[Dy_6Cu_6(H_2L')_6Cl_{12}(H_2O)_6] \cdot 4Cl \cdot 2OH \cdot 39H_2O$ (H_2L' – N-donor ligand with multiple coordination sites). SMM behavior was observed under the applied dc field as a result of Dy· · ·Cu magnetic coupling.

In 2004, Geim and Novoselov from the University of Manchester isolated graphene, although existence of this carbon allotrope was foreseen many years before [137]. In 2010, this discovery was recognized with a Nobel Prize in physics. For the first time graphene was mechanically exfoliated from small mesas of highly oriented pyrolytic graphite in the form of stable layers with thickness of few atoms or even single layers. Graphene is 200 times stronger than steel, almost transparent, and electrically conductive. Interestingly, for its first isolation a simple adhesive tape was used. The "miracle material" was expected to revolutionize molecular electronics.

Yao and coworkers [133] proposed an efficient filter and spin valve comprising an $[Fe_4]$ SMM between two graphene electrodes. The computational studies of such junction indicate that its efficiency should approach 100% and there is a strong dependence of a spin-polarized transport on the molecular spin alignment. The $[Fe_4(OMe)_6(dpm)_6]$ (dpm = dipivaloylmethane) cluster is used for its stable magnetic properties and graphene electrodes help to overcome the oxidation of metallic contacts and unstable molecule/electrodes interface in case of the use of metallic electrodes.

Lumetti et al. [138] combined nanometer-separated graphene electrodes with $TbPc_2$ SMM to fabricate novel cryogenic spintronic devices by feedback-controlled electroburning. This procedure is based on the reaction of carbon atoms with oxygen at high temperatures resulting from Joule heating at large current densities. The new molecular devices were subject to electrical transport measurements and in 17.5% of them Coulomb blockade-like features were observed. The Pc ligands were found to create a quantum dot in the vicinity of the Tb^{3+} spin. In one case, the authors were able to estimate the nature and magnitude of the Pc–Tb exchange interaction.

Islam and Benjamin [139] examined the effect of adiabatic twisting of a $Tb(Pc)_2$ molecule embedded in a graphene monolayer. Adiabatic quantum pumping is defined as charge/spin carriers transfer achieved by a cyclic change of two independent system parameters without application of any external perturbation, e.g. voltage bias. The authors show that through adiabatic quantum pumping pure spin currents can be generated in the investigated system.

Er-based SMM, Er(trensal) (H_3trensal = 2,2′,2″-tris(salicylideneimino)triethylamine), was adsorbed on graphene/Ru(0001), graphene/Ir(111), and bare Ru(0001) surfaces by Dreiser et al. [140]. It was found that on graphene the SMM molecules tend to form dense islands with their magnetic easy axes oriented perpendicular to the surface. On bare Ru(0001) the alignment of the magnetic easy axes is weak and no distinct ordering of the complex molecules is observed. These phenomena were monitored with STM, XAS, and XMCD techniques. Thus a demonstration of control of the net magnetic anisotropy within a molecule–inorganic heterostructure was achieved.

Yamashita and coworkers [141] constructed a molecular machine where salene-chelated mononuclear Mn(III) SMMs are joined with a photoswitchable

ligand and thus their magnetic properties are activated with visible light that could be used to design new memory devices. The applied ligands were photoactive derivatives of diarylethene with two hydroxo groups, capable of reversible isomerization to "open" and "closed" forms upon irradiation with UV/Vis light. For the assembly with the "closed" form of the ligand, no slow relaxation of magnetization was observed, whereas for the "open" form the SMM behavior was "switched on." The effect was attributed to the interplay of two factors: (i) change in inter- and intramolecular Mn· · ·Mn distances, (ii) delocalization of thiophene π-electron density over the ligand molecule in the "closed" form.

A conducive factor for the application of SMMs in solid state devices seems to be their organization on surfaces. Within this arrangement the local anisotropy of SMMs must be controlled and it must be ensured that they retain their specific magnetic properties. Mannini and coworkers [142] demonstrated that low-temperature MFM can be used as an alternative to less accessible laboratory-based magnetometric techniques for XMCD investigation. $TbPc_2$/PTCDA (PTCDA = perylene-3,4,9,10-tetracarboxylic dianhydride) model nanosized films on SiO_2 were investigated and shown to yield analogous results as obtained by XMCD. The molecular orientation of the $Tbpc_2$ SMM was engineered by means of control of the molecule–substrate interactions, where PTCDA was used initially as a templating agent, known to direct phthalocyanine rings to coplanar position.

1.3.6 Magnetic Refrigerants

Magnetic refrigeration is another interesting prospective application of molecular magnets [143]. This technology could help to tackle such challenges as environmental issues – a gas-free and economic process with reduction in energy consumption and increase in efficiency. A unique feature in the case of molecular magnets is operation under low temperatures which could be a low-cost alternative to helium-3. Magnetic refrigeration is characterized by the magnetocaloric effect (MCE). MCE is defined as change of ΔS_m (isothermal magnetic anisotropy) and ΔT_{ad} (change of adiabatic temperature) with change of the applied magnetic field [144]. For large ΔS_m values, particularly M vs H data allow to evaluate the MCE by determination of ΔS_m using the Maxwell equation:

$$\Delta S_m(T) = \int [\partial M(T,H)/\partial T]_H \mathrm{d}H$$

The most common magnetic refrigerants so far are gadolinium(III) complexes. The isotropic Gd(III) spins assist a large change of the magnetic entropy and adiabatic temperature on change in the applied magnetic field. In polynuclear metal complexes in general the desirable species are high-spin isotropic compounds with weak intramolecular magnetic exchange. This led to the discovery of such magnetic refrigerants as the $[Fe_{14}]$ cluster [145–147], supertetrahedron $[Mn_{10}]$ [148] or disk-like $[Mn_{14}]$ complex [149].

Cui, Zhao, and coworkers [150] reported on a series of lanthanide(III) dinuclear complexes with an 8-hydroxyquinoline Schiff-base derivative as a bridging ligand. The general formula for these compounds is $[Ln_2(hfac)_4(L)_2]$ (Ln(III) = Gd (**1**),

Tb (**2**), Dy (**3**), Ho (**4**), Er (**5**)), $[Ln_2(tfac)_4(L)_2]$ (Ln(III) = Gd (**6**), Tb (**7**), Dy (8), Ho (**9**)), and $[Dy(bfac)_4(L)_2{\cdot}C_7H_{16}]$ (**10**) (L = 2-[[(4-fluorophenyl)imino] methyl]-8-hydroxyquinoline, hfac = hexafluoroacetylacetonate, tfac = trifluoroacetylacetonate, and bfac = benzoyltrifluoroacetone). The Gd complexes **1**, **6** of both formulae display cryogenic magnetic refrigeration properties, whereas **3**, **7**, **8**, and **10** are SMMs.

Konar and coworkers [144] performed a lanthanide-directed synthesis of four tetranuclear quadruple-stranded helicates showing magnetic refrigeration and SMM behavior. These rare-topology compounds are characterized by the following formulae: $[Ln_4L_4(OH)_2](OAc)_2 \cdot xH_2O$ (Ln = Gd^{III}, Dy^{III} and $x = 4$, 5, respectively), $[Er_4L_4(OH)_2](NO_3)_2 \cdot 9H_2O$, and $[Dy_4L_4(NO_3)](NO_3)_2 \cdot 2CH_3OH \cdot H_2O$ with H_2L = butanedihydrazide-bridged bis(3-ethoxysalicylaldehyde) ligand.

Evangelisti, Dalgarno, Brechin, and coworkers [151] introduced a new family of 3d/4f metal complexes employing for the first time methylene-bridged calix[4]arene ligands. In the family of clusters of the formula $[Mn^{III}{}_4Ln^{III}{}_4(OH)_4(C4)_4(NO_3)_2(DMF)_6(H_2O)_6](OH)_2$ (where C4 = calix[4]arene; Ln = Gd, Tb, Dy) the Tb/Dy complexes are SMMs and the Gd complex is a magnetic refrigerant. This property of the Gd complex arises due to its low anisotropy that facilitates facile polarization of the net molecular spin, as well as the presence of low-lying excited spin states, that adds to the resulting magnetic entropy.

Bendix and coworkers [152] reported on the presence of magnetic refrigerants in the series of labile, fluoride-bridged $[Gd^{III}{}_3M^{III}{}_2]$ (M = Cr, Fe, Ga) complexes. A reaction of $Gd(NO_3)_3 \cdot 5H_2O$ with *fac*-$[CrF_3(Me_3tacn)] \cdot 4H_2O$ (Me_3tacn = *N,N′,N″*-trimethyl-1,4,7-triazacyclononane) led to the $[\{CrF_3(Me_3tacn)\}_2Gd_3F_2(NO_3)_7(H_2O)(CH_3CN)] \cdot 4CH_3CN$ complex. Use of *fac*-$[FeF_3(Me_3tacn)] \cdot H_2O$ and *fac*-$GaF_3(Me_3tacn)] \cdot 4H_2O$ led to isostructural $[\{MF_3(Me_3tacn)\}_2Gd_3F_2(NO_3)_7(H_2O)(CH_3CN)] \cdot 4CH_3CN$ (M = Fe, Ga) complexes of Fe and Ga, respectively. For these complexes, weak exchange interactions were rationalized computationally. For the Cr and Fe analogues, large magnetic entropy changes of 38.3 and 33.1 J $(kg{\cdot}K)^{-1}$ were found, respectively, on change in field from 7 to 0 T. The differences between these complexes led to the conclusion that engineering of the close-lying excited states should be an important part of a magnetic refrigerant design.

Large MCE was also reported by Kong, Long, and coworkers [153] for the record-nuclearity keplerate $[Gd_{104}]$ compound, $[Gd_{104}(ClO_4)_6(CH_3COO)_{56}(\mu_3\text{-}OH)_{168}(\mu_4O)_{30}(H_2O)_{112}](ClO_4)_{22} \cdot (CH_3CH_2OH)_2 \cdot 140H_2O$, one of the series, along with the related Nd complex. The complex, with large metal/ligand ratio, was self-assembled in hydrolysis of a mixture containing $Gd(ClO_4)_3$, $Co(CH_3COO)_2 \cdot 4H_2O$ and *N*-acetyl-D-glucosamine.

Studies of a model magnetic refrigerant on deposition on a surface were recently undertaken by Affronte and coworkers [154]. The chosen model compound was $[Fe_{14}(bta)_6O_6(OMe)_{18}Cl_6]$ (bta = benzotriazole), deposited on a gold surface from a liquid phase. A number of surface analysis techniques (STM, X-ray photoelectron spectroscopy (XPS), XAS, XMCD) were employed in this study. It was shown that at the applied concentration range the complex molecules do not aggregate, but retain their chemical and structural integrity, as

well as their capabilities as magnetic refrigerants. This proves that at least in this case the down-scaling of devices for magnetic refrigeration should be possible.

A very original approach was recently developed by Evangelisti and coworkers [155]. In contrast to the widespread research on magnetically isotropic refrigerants, it was shown that dysprosium acetate tetrahydrate, $[\{Dy(OAc)_3(H_2O)_2\}_2]\cdot 4H_2O$, may also be used for cooling below the temperature of liquid helium. The effect was achieved through rotation of aligned single crystals in a constant applied magnetic field. In a cryogenic adiabatic demagnetization refrigerator a magnetic field of few teslas is applied through a superconducting magnet and removed in a cycle. The speed of the field removal is a limiting factor connected with irreversible heat flows. However, it was already shown that the time of field removal can be reduced from the order of minutes to seconds by using rotating aligned single crystals of anisotropic $HoMn_2O_5$ and $KEr(MoO_4)_2$ [156, 157]. The authors envisage more such examples in the future, leading to the advent of compact refrigerants based on large single crystals of dysprosium acetate or their oriented aggregates.

Tang and coworkers [158] showed that the MCE can be enhanced for a $[Gd_4(\mu_4\text{-}O)L_2(PhCOO)_6]$·solvent complex ($H_2L$ = a bi-Schiff-based ligand) via absorption of atmospheric carbon dioxide, leading to an assembly of $[Gd_8(\mu_3\text{-}OH)_4(CO_3)_2L_4(PhCOO)_8]$·solvent product. The authors speculated that this enhancement may be due to the weak ferromagnetic interaction transmitted through carbonate bridges.

1.3.7 Applications in Other Disciplines

The interdisciplinary character of the field of SMM science is underlined by the numerous applications in very different areas. For instance, in biology, SMMs as polynuclear metal complexes can be used to model active centers of enzymes. The superparamagnet-like behavior of metal nanoparticles used for drug delivery is anticipated to be transferable to real analogous applications of SMMs.

$[Mn_{12}]$-based contrasting agents have been considered as an alternative to gadolinium-based agents for peripheral vascular and coronary artery disease due to its possible involvement in cases of nephrogenic systemic fibrosis [159]. A clear limitation is the poor solubility and stability in water. To overcome this, $[Mn_{12}]$ molecules were grafted on polystyrene beads [160, 161]. Moreover, a possibility to create an emulsion with $[Mn_{12}]$ clusters with acetate ligands exchanged with stearate ligands was considered [160, 161]. Another strategy was to create micellar polymeric particles of sub-20 nm size, based on $[Mn_{12}]$, which are well-defined and capable of penetrating minuscule blood vessels [159]. This approach is again based on carboxylate substitution with amphiphilic ligands in the $[Mn_{12}]$ core. Such micelles have already been successfully tested in vivo as magnetic resonance imaging (MRI) agents on a rat model. A significant MRI contrast enhancement was detected for rat heart, liver, and kidney.

In general, SMMs with large molecular size and often aesthetically pleasing molecular architectures are considered as representatives of nanomaterials relevant for nanotechnology. The relevant sizes are from 1 to 1000 nm and cover not only magnetic, but also semiconductor materials (quantum dots)

or carbon nanostructures, such as CNTs. These materials already find many applications due to their unique properties but there is an ongoing discussion about their possible toxicological impact as no long-term studies are available yet. In the field of SMMs recently Christou, Stamatatos, and coworkers [162] reported on a new spherical $[Mn_{29}]$ molecular cluster with dimensions of ca. 2.2 nm, comparable to smallest magnetic nanoparticles. The compound was obtained in a comproportionation reaction between Mn(II) and Mn(VII) starting compounds in the presence of 3,3-dimethylacrylic acid incorporated in the resulting product. The same group also concurrently reported on two large molecular toruses, $[Mn_{70}O_{60}(O_2CMe)_{70}(OEt)_{20}(EtOH)_{16}(H_2O)_{22}]$ and $[Mn_{70}O_{60}(O_2CMe)_{70}(OC_2H_4Cl)_{20}(ClC_2H_4OH)_{18}(H_2O)_{22}]$, of ca. 4 nm diameter, crystallizing in stacks to assemble "supramolecular tubes." These SMMs displayed hysteresis loops at temperatures below 1.5 K and energy barriers of 23 and 18 K, respectively. Studies with both classical (Néel–Brown) and quantum approach were both successful in validating the experimental values and showed that the molecules are situated at the quantum-classical nanoparticle interface. The $[Mn_{70}]$ compounds were obtained as a result of alcoholysis of the $[Mn_{12}]$ starting compound in the presence of EtOH and 2-ClC_2H_4OH, respectively. Reaction systems related to those that yielded the $[Mn_{29}]$ and $[Mn_{70}]$ products have been previously shown to often yield large manganese clusters and are likely to produce more in the future.

Another realized direction is adding other properties to the SMM-based materials. These could be e.g. porosity, opening a way toward application in gas storage. A good example is from the study published by Kou and coworkers [163] on porous coordination polymers based on $[Mn_6]$ SMMs. Three isostructural compounds, $[Mn_6(\mu_3\text{-}O)_2(sao)_6(DMF)_4(L^1)_{2/3}]\cdot 4DMF\cdot 2H_2O\cdot 2CH_3OH$, $[Mn_6(\mu_3\text{-}O)_2(sao)_6(DMF)_4(L^2)_{2/3}]\cdot 4DMF\cdot 2H_2O\cdot 2CH_3OH$, and $[Mn_6(\mu_3\text{-}O)_2(sao)_6\text{-}(DMF)_4(L^3)_{2/3}]\cdot 4DMF\cdot 4H_2O\cdot 2CH_3OH$ (DMF = dimethylformamide, H_2sao = salicylaldoxime, H_3L^1 = benzene-1,3,5-trisbenzoic acid, H_3L^2 = 4,4′,4″-*s*-triazine-2,4,6-triyltribenzoic acid, and H_3L^3 = 2,4,6-tris(4-carboxyphenoxy)-1,3,5-*s*-triazine), derived from classical oxime-bridged $[Mn_6]$ SMMs, were synthesized. These materials show not only SMM behavior but also selective absorption of CO_2 over N_2 at 273 K.

Applications of SMMs can be extended even further when their specific magnetic properties occur simultaneously with such useful photophysical properties as fluorescence. Such multifunctional SMMs could be used as switches or sensors under different conditions. Lanthanide-based SMMs can potentially display optical properties useful in organic light-emitting diodes (OLEDs), bioimaging, time-resolved luminescent immunoassays, and imaging spectroscopy [164].

For instance, Gao, Cui et al. [165] used 8-hydroxyquinolinate ligand to introduce further useful photophysical properties to lanthanide-based SMMs. Derivatives of quinoline are known to be luminescent/electroluminescent and also for their applications in nonlinear optics. In particular, their lanthanide complexes are promising as constituents of electroluminescent devices. Gao, Cui et al. studied also the magnetic behavior of such compounds, pointing the observed SMM behavior as an additional property potentially broadening the

scope of such devices. Five tetranuclear complexes, $[RE_4(dbm)_4L_6(\mu_3-OH)_2]$ (HL = 5-(4-fluorobenzylidene)-8-hydroxylquinoline; dbm = 1,3-diphenyl-1,3-propanedione; RE = Y, Eu, Tb, Dy, Lu) of butterfly/rhombus topology, were reported. The Dy complex turned out to be an SMM under a zero dc field with the blocking temperature of 10 K and the effective energy barrier to spin reversal at 56 K.

Pinkowicz, Yamashita, et al. [166] reported on a series of 2D lanthanide-based coordination polymers displaying a photocontrolled SMM behavior. This was achieved by the use of a photoactive ligand, 1,2-bis(5-carboxyl-2-methyl-3-thienyl)perfluorocyclopentene (dae^{2-}) to obtain $[\{Ln^{III}_2(dae)_3(DMSO)_3(MeOH)\}]\cdot 10\ MeOH]_n$ (Ln = Dy, Ho) complexes. The Dy complex was found to be an SMM, undergoing a UV-light-induced ligand isomerization which was shown to affect its magnetic properties. Apparently, the thus-induced changes in the Dy^{3+} ions coordination sphere and, as a consequence, the magnetic easy axis, affected the relaxation of magnetization through quantum tunneling. The changes in the magnetic properties turned out to be irreversible.

A frequent limitation of the practical applications of SMMs, their instability, was overcome by Wang, Gao, and coworkers [167] with the synthesis of rare, thermostable, sublimable, photoluminescent Dy(III)-based SMMs. The compounds are mononuclear ($[ADyL_4]\cdot[solvent]$) with a naphthyridine-like ligand (L = 4-hydroxy-8-methyl-1,5-naphthyridine-3-carbonitrile) and alkali metal ions (A = Na, K, Rb, Cs). These compounds are SMMs with effective energy barriers to spin reversal at ca. 137 K under a zero dc field. The stability of these compounds upon sublimation was confirmed with powder diffraction. Studies of the magnetic properties indicated that also their SMM behavior was retained.

Another aspect is the possibility to manipulate SMMs and to place them in matrices without bias to their specific magnetic properties. Such a feature has recently been reported by Mallah, Mialane, and coworkers [168] for an $[(FeW_9O_{34})_2Fe_4(H_2O)_2]^{10-}$ POM. Both direct and post-synthetic approaches could be employed to incorporate these molecules in a biopolymer gelatin matrix. Moreover, other matrices used successfully in this study included diamagnetic and antiferromagnetic metal–organic frameworks: UiO-67 and MIL-101(Cr), respectively. Interestingly, the SMM property is fully retained in the biopolymer matrix and fully corresponds to the values recorded for the pure SMM in crystalline state. In the diamagnetic metal-organic framework (MOF) a slight decrease in the energy barrier is observed, whereas placement in a paramagnetic MOF obviously results in additional magnetic interactions, reduction in hysteresis loops, and smearing of the quantum tunneling steps.

Pointillart et al. [164] decided to explore a combination of the photophysical properties of lanthanides with electronic properties of the tetrathiafulvalene (TTF)-based ligands. The TTF derivatives are known for their use in such conducting materials as organic conductors, semiconductors, and superconductors. The authors used TTF ligands functionalized with a differing number of oxygenated/nitrogenated acceptor moieties coordinating to lanthanide ions. The starting lanthanide complexes were either with hexafluoroacetylacetonate or 2-thenoyltrifluoroacetylacetonate ligands. The role played by the TTF-based

ligands was twofold: to isolate the magnetic centers and to sensitize them as an organic chromophore. The resulting products displayed both visible/near infrared (NIR) lanthanide luminescence and SMM behavior. In particular, addition of 3d metals to obtain heterobimetallic assemblies could extend their functionality even more, e.g. with the thermal spin crossover or light-induced excited spin-state trapping (LIESST) properties.

Particularly valuable with respect to sensing/magnetic switching applications are SMMs in which a switch of the magnetic properties is accompanied by change in other properties. For instance, Pardo, Cano, and coworkers [169] published this effect for SIMs. Mononuclear Co(II) complexes, $[Co^{II}(dmbpy)_2](ClO_4)_2$ and $[Co^{II}(dmbpy)_2(H_2O)](ClO_4)_2$ (dmbpy = 6,6′-dimethyl-2,2′-bipyridine), were investigated, displaying a reversible coordination of a water molecule. The hydrated form with "fast-relaxing" magnetization (no SIM property) was reported to be orange, whereas upon water loss a deep red "slow-relaxing" form (SIM property) was obtained. The phenomenon was explained in terms of local sterically constrained environment, reminiscent of the natural enzymes "entatic" state. The switch of optical/magnetic properties is dependent on the relative humidity and temperature of the environment.

Pointillart, Crassous, Le Guennic, and coworkers [170] combined SIM property of Dy^{3+} ions with chiral [6]-helicene ligands to obtain chiral SMMs. Chirality may help in future applications where enantioselectivity plays a role, e.g. in stereospecific transport of drug molecules in living organisms or, specifically for lanthanide complexes, circularly polarized luminescence. The investigated complexes were reported to display a significant difference in the magnetic properties of the racemic and enantiopure forms: the (+) form was found to be ferromagnetic with more pronounced SMM behavior than the antiferromagnetic racemic form in solid state.

Acknowledgment

Help of Dejan Premuzic with preparation of the figures and formatting of the references is acknowledged.

References

1 Ako, A.M., Mereacre, V., Clérac, R. et al. (2009). A $[Mn_{18}Dy]$ SMM resulting from the targeted replacement of the central Mn^{II} in the $S = 83/2$ $[Mn_{19}]$-aggregate with Dy^{III}. *Chem. Commun.* (5): 544–546.

2 Mereacre, V., Akhtar, M.N., Lan, Y. et al. (2010). Structures and magnetic properties of $Mn^{III}{}_4Ln^{III}{}_4$ aggregates with a "square-in-square" topology. *Dalton Trans.* 39 (20): 4918–4927.

3 Glauber, R.J. (1963). Time-dependent statistics of the Ising model. *J. Math. Phys.* 4 (2): 294–307.

4 Caneschi, A., Gatteschi, D., Lalioti, N. et al. (2001). Cobalt(II)-nitronyl nitroxide chains as molecular magnetic nanowires. *Angew. Chem. Int. Ed.* 40 (9): 1760–1763.

5 Miyasaka, H., Nezu, T., Sugimoto, K. et al. (2005). $[Mn^{III}_2$ (5-Rsaltmen)$_2$ $Ni^{II}(pao)_2(L)]^{2+}$: an $S(T) = 3$ building block for a single-chain magnet that behaves as a single-molecule magnet. *Chem. Eur. J.* 11 (5): 1592–1602.

6 Sun, H.-L., Wang, Z.-M., and Gao, S. (2010). Strategies towards single-chain magnets. *Coord. Chem. Rev.* 254 (9–10): 1081–1100.

7 Dhers, S., Feltham, H.L.C., and Brooker, S. (2015). A toolbox of building blocks, linkers and crystallisation methods used to generate single-chain magnets. *Coord. Chem. Rev.* 296: 24–44.

8 Cassaro, R.A.A., Reis, S.G., Araujo, T.S. et al. (2015). A single-chain magnet with a very high blocking temperature and a strong coercive field. *Inorg. Chem.* 54 (19): 9381–9383.

9 Wei, R.-M., Cao, F., Li, J. et al. (2016). Single-chain magnets based on octa-cyanotungstate with the highest energy barriers for cyanide compounds. *Sci. Rep.* 6: 24372 1–8.

10 Zhang, Y.-Z., Zhao, H.-H., Funck, E., and Dunbar, K.R. (2015). A single-chain magnet tape based on hexacyanomanganate(III). *Angew. Chem. Int. Ed.* 54 (19): 5583–5587.

11 Ishikawa, N., Sugita, M., Ishikawa, T. et al. (2003). Lanthanide double-decker complexes functioning as magnets at the single-molecular level. *J. Am. Chem. Soc.* 125 (29): 8694–8695.

12 Westerstro, R., Dreiser, J., Piamonteze, C. et al. (2012). An endohedral single-molecule magnet with long relaxation times: DySc2N@C80. *J. Am. Chem. Soc.* 134: 9840–9843.

13 Rinehart, J.D., Fang, M., Evans, W.J., and Long, J.R. (2011). Strong exchange and magnetic blocking in N_2^{3-}-radical-bridged lanthanide complexes. *Nat. Chem.* 3 (7): 538–542.

14 Frost, J.M., Harriman, K.L.M., and Murugesu, M. (2016). The rise of 3-d single-ion magnets in molecular magnetism: towards materials from molecules? *Chem. Sci.* 7 (4): 2470–2491.

15 Vallejo, J., Pascual-Álvarez, A., Cano, J. et al. (2013). Field-induced hysteresis and quantum tunneling of the magnetization in a mononuclear manganese(III) complex. *Angew. Chem. Int. Ed.* 52 (52): 14075–14079.

16 Ishikawa, R., Miyamoto, R., Nojiri, H. et al. (2013). Slow relaxation of the magnetization of an Mn^{III} single ion. *Inorg. Chem.* 52 (15): 8300–8302.

17 Pascual-Álvarez, A., Vallejo, J., Pardo, E. et al. (2015). Field-induced slow magnetic relaxation in a mononuclear manganese(III)-porphyrin complex. *Chem. Eur. J.* 21 (48): 17299–17307.

18 Rechkemmer, Y., Breitgoff, F.D., van der Meer, M. et al. (2016). A four-coordinate cobalt(II) single-ion magnet with coercivity and a very high energy barrier. *Nat. Commun.* 7: 10467 1–8.

19 Karasawa, S., Zhou, G., Morikawa, H., and Koga, N. (2003). Magnetic properties of tetrakis[4-(α-diazobenzyl)pyridine]bis(thiocyanato-N)cobalt(II) in

frozen solution after irradiation. Formation of a single-molecule magnet in frozen solution. *J. Am. Chem. Soc.* 125 (45): 13676–13677.

20 Novikov, V.V., Pavlov, A.A., Nelyubina, Y.V. et al. (2015). A trigonal prismatic mononuclear cobalt(II) complex showing single-molecule magnet behavior. *J. Am. Chem. Soc.* 137 (31): 9792–9795.

21 Habib, F., Luca, O.R., Vieru, V. et al. (2013). Influence of the ligand field on slow magnetization relaxation versus spin crossover in mononuclear cobalt complexes. *Angew. Chem. Int. Ed.* 52 (43): 11290–11293.

22 Zadrozny, J.M. and Long, J.R. (2011). Slow magnetic relaxation at zero field in the tetrahedral complex $[Co(SPh)_4]^{2-}$. *J. Am. Chem. Soc.* 133 (51): 20732–20734.

23 Zadrozny, J.M., Telser, J., and Long, J.R. (2013). Slow magnetic relaxation in the tetrahedral cobalt(II) complexes $[Co(EPh)_4]^{2-}$ (E = O, S, Se). *Polyhedron* 64: 209–217.

24 Fataftah, M.S., Zadrozny, J.M., Rogers, D.M., and Freedman, D.E. (2014). A mononuclear transition metal single-molecule magnet in a nuclear spin-free ligand environment. *Inorg. Chem.* 53 (19): 10716–10721.

25 Ziegenbalg, S., Hornig, D., Görls, H., and Plass, W. (2016). Cobalt(II)-based single-ion magnets with distorted pseudotetrahedral $[N_2O_2]$ coordination: experimental and theoretical investigations. *Inorg. Chem.* 55 (8): 4047–4058.

26 Poulten, R.C., Page, M.J., Algarra, A.G. et al. (2013). Synthesis, electronic structure, and magnetism of $[Ni(6\text{-}Mes)_2]^+$: a two-coordinate nickel(I) complex stabilized by bulky N-heterocyclic carbenes. *J. Am. Chem. Soc.* 135 (37): 13640–13643.

27 Marriott, K.E.R., Bhaskaran, L., Wilson, C. et al. (2015). Pushing the limits of magnetic anisotropy in trigonal bipyramidal Ni(II). *Chem. Sci.* 6 (12): 6823–6828.

28 Miklovič, J., Valigura, D., Boča, R., and Titiš, J. (2015). A mononuclear Ni(II) complex: a field induced single-molecule magnet showing two slow relaxation processes. *Dalton Trans.* 44 (28): 12484–12487.

29 Deng, Y.F., Han, T., Wang, Z. et al. (2015). Uniaxial magnetic anisotropy of square-planar chromium(II) complexes revealed by magnetic and HF-EPR studies. *Chem. Commun.* 51 (100): 17688–17691.

30 Ding, M., Cutsail, G.E., Aravena, D. et al. (2016). A low spin manganese(IV) nitride single molecule magnet. *Chem. Sci.* 7: 6132–6140.

31 Liu, J., Chen, Y.-C., Liu, J.-L. et al. (2016). A stable pentagonal bipyramidal Dy(III) single-ion magnet with a record magnetization reversal barrier over 1000 K. *J. Am. Chem. Soc.* 138 (16): 5441–5450.

32 Ding, Y.-S., Chilton, N.F., Winpenny, R.E.P., and Zheng, Y.-Z. (2016). On approaching the limit of molecular magnetic anisotropy: a near-perfect pentagonal bipyramidal dysprosium(III) single-molecule magnet. *Angew. Chem. Int. Ed.* 55 (52): 16071–16074.

33 Chibotaru, L.F., Ungur, L., and Soncini, A. (2008). The origin of nonmagnetic Kramers doublets in the ground state of dysprosium triangles: evidence for a toroidal magnetic moment. *Angew. Chem. Int. Ed.* 47 (22): 4126–4129.

34 Ungur, L., Lin, S.-Y., Tang, J., and Chibotaru, L.F. (2014). Single-molecule toroics in Ising-type lanthanide molecular clusters. *Chem. Soc. Rev.* 43 (20): 6894–6905.

35 Novitchi, G., Pilet, G., Ungur, L. et al. (2012). Heterometallic Cu^{II}/Dy^{III} 1D chiral polymers: chirogenesis and exchange coupling of toroidal moments in trinuclear Dy_3 single molecule magnets. *Chem. Sci.* 3 (4): 1169–1176.

36 Guo, P.-H., Liu, J.-L., Zhang, Z.-M. et al. (2012). The first $\{Dy_4\}$ single-molecule magnet with a toroidal magnetic moment in the ground state. *Inorg. Chem.* 51 (3): 1233–1235.

37 Tang, J., Hewitt, I., Madhu, N.T. et al. (2006). Dysprosium triangles showing single-molecule magnet behavior of thermally excited spin states. *Angew. Chem. Int. Ed.* 45 (11): 1729–1733.

38 Lin, S.-Y., Wernsdorfer, W., Ungur, L. et al. (2012). Coupling Dy_3 triangles to maximize the toroidal moment. *Angew. Chem. Int. Ed.* 51 (51): 12767–12771.

39 Lis, T. (1980). Preparation, structure, and magnetic properties of a dodecanuclear mixed-valence manganese carboxylate. *Acta Cryst.* 36 (9): 2042–2046.

40 Weinland, R.F. and Fischer, G. (1921). Über Manganiacetate und -benzoate. *Z. Anorg. Allg. Chem.* 120 (1): 161–180.

41 Wieghardt, K., Pohl, K., Jibril, I., and Huttner, G. (1984). Hydrolysis products of the monomeric amine complex $(C_6H_{15}N_3)FeCl_3$: the structure of the octameric iron(III) cation of $\{[(C_6H_{15}N_3)_6Fe_8(\mu_3\text{-}O)_2(\mu_2\text{-}OH)_{12}]Br_7(H_2O)\}Br{\cdot}8H_2O$. *Angew. Chem. Int. Ed. Engl.* 23 (1): 77–78.

42 Milios, C.J., Vinslava, A., Wernsdorfer, W. et al. (2007). A record anisotropy barrier for a single-molecule magnet. *J. Am. Chem. Soc.* 129 (10): 2754–2755.

43 Katoh, K., Yoshida, Y., Yamashita, M. et al. (2009). Direct observation of lanthanide(III)-phthalocyanine molecules on Au(111) by using scanning tunneling microscopy and scanning tunneling spectroscopy and thin-film field-effect transistor properties of Tb(III)- and Dy(III)-phthalocyanine molecules. *J. Am. Chem. Soc.* 131 (29): 9967–9976.

44 Rinehart, J.D., Fang, M., Evans, W.J., and Long, J.R. (2011). A N_2^{3-} radical-bridged terbium complex exhibiting magnetic hysteresis at 14 K. *J. Am. Chem. Soc.* 133 (36): 14236–14239.

45 Hoeke, V., Heidemeier, M., Krickemeyer, E. et al. (2012). Environmental influence on the single-molecule magnet behavior of $[Mn^{III}_6Cr^{III}]^{3+}$: molecular symmetry versus solid-state effects. *Inorg. Chem.* 51 (20): 10929–10954.

46 Caneschi, A., Gatteschi, D., Sessoli, R. et al. (1991). Alternating current susceptibility, high field magnetization, and millimeter band EPR evidence for a ground $S = 10$ state in $[Mn_{12}O_{12}(CH_3COO)_{16}(H_2O)_4]{\cdot}2CH_3COOH{\cdot}4H_2O$. *J. Am. Chem. Soc.* 113 (15): 5873–5874.

47 Sessoli, R., Tsai, H.L., Schake, A.R. et al. (1993). High-spin molecules: $[Mn_{12}O_{12}(O_2CR)_{16}(H_2O)_4]$. *J. Am. Chem. Soc.* 115 (5): 1804–1816.

48 Eppley, H.J., Tsai, H.-L., de Vries, N. et al. (1995). High-spin molecules: unusual magnetic susceptibility relaxation effects in $[Mn_{12}O_{12}(O_2CEt)_{16}(H_2O)_3]$ ($S = 9$) and the one-electron reduction product $(PPh_4)[Mn_{12}O_{12}(O_2CEt)_{16}(H_2O)_4]$ ($S = 19/2$). *J. Am. Chem. Soc.* 117 (1): 301–317.

49 Chakov, N.E., Soler, M., Wernsdorfer, W. et al. (2005). Single-molecule magnets: structural characterization, magnetic properties, and ^{19}F NMR spectroscopy of a Mn_{12} family spanning three oxidation levels. *Inorg. Chem.* 44 (15): 5304–5321.

50 Hill, S., Anderson, N., Wilson, A. et al. (2005). A comparison between high-symmetry Mn_{12} single-molecule magnets in different ligand/solvent environments. *Polyhedron* 24 (16–17): 2284–2292.

51 Chi-Dong Park, D.-Y.J. (2001). Soluble single-molecule magnet: Mn_{12}-stearate. *Bull. Korean Chem. Soc.* 22 (6): 611–615.

52 Zhao, H., Berlinguette, C.P., Bacsa, J. et al. (2004). Structural characterization, magnetic properties, and electrospray mass spectrometry of two Jahn–Teller isomers of the single-molecule magnet $[Mn_{12}O_{12}(CF_3COO)_{16}(H_2O)_4]$. *Inorg. Chem.* 43 (4): 1359–1369.

53 Burgert, M., Voss, S., Herr, S. et al. (2007). Single-molecule magnets: a new approach to investigate the electronic structure of Mn_{12} molecules by scanning tunneling spectroscopy. *J. Am. Chem. Soc.* 129 (46): 14362–14366.

54 Cornia, A., Fabretti, A.C., Pacchioni, M. et al. (2003). Direct observation of single-molecule magnets organized on gold surfaces. *Angew. Chem. Int. Ed.* 42 (14): 1645–1648.

55 Pacchioni, M., Cornia, A., Fabretti, A.C. et al. (2004). Site-specific ligation of anthracene-1,8-dicarboxylates to an Mn_{12} core: a route to the controlled functionalisation of single-molecule magnets. *Chem. Commun.* (22): 2604–2605.

56 Bagai, R. and Christou, G. (2009). The *Drosophila* of single-molecule magnetism: $[Mn_{12}O_{12}(O_2CR)_{16}(H_2O)_4]$. *Chem. Soc. Rev.* 38 (4): 1011–1026.

57 Friedman, J.R., Sarachik, M.P., Tejada, J., and Ziolo, R. (1996). Macroscopic measurement of resonant magnetization tunneling in high-spin molecules. *Phys. Rev. Lett.* 76 (20): 3830–3833.

58 Hernández, J.M., Zhang, X.X., Luis, F. et al. (1996). Field tuning of thermally activated magnetic quantum tunnelling in Mn_{12} − Ac molecules. *Europhys. Lett.* 35 (4): 301–306.

59 Thomas, L., Lionti, F., Ballou, R. et al. (1996). Macroscopic quantum tunnelling of magnetization in a single crystal of nanomagnets. *Nature* 383 (6596): 145–147.

60 Delfs, C., Gatteschi, D., Pardi, L. et al. (1993). Magnetic properties of an octanuclear iron(III) cation. *Inorg. Chem.* 32 (14): 3099–3103.

61 Sangregorio, C., Ohm, T., Paulsen, C. et al. (1997). Quantum tunneling of the magnetization in an iron cluster nanomagnet. *Phys. Rev. Lett.* 78 (24): 4645–4648.

62 Gatteschi, D. and Sessoli, R. (2003). Quantum tunneling of magnetization and related phenomena in molecular materials. *Angew. Chem. Int. Ed.* 42 (3): 268–297.

63 Gatteschi, D., Sessoli, R., and Cornia, A. (2000). Single-molecule magnets based on iron(III) oxo clusters. *Chem. Commun.* (9): 725–732.

64 Milios, C.J., Raptopoulou, C.P., Terzis, A. et al. (2004). Hexanuclear manganese(III) single-molecule magnets. *Angew. Chem. Int. Ed.* 43 (2): 210–212.

65 Ako, A.M., Hewitt, I.J., Mereacre, V. et al. (2006). A ferromagnetically coupled Mn_{19} aggregate with a record $S = 83/2$ ground spin state. *Angew. Chem. Int. Ed.* 45 (30): 4926–4929.

66 Ishikawa, N., Sugita, M., Okubo, T. et al. (2003). Determination of ligand-field parameters and f-electronic structures of double-decker bis(phthalocyaninato)lanthanide complexes. *Inorg. Chem.* 42 (7): 2440–2446.

67 Ganivet, C.R., Ballesteros, B., de, la Torre, G. et al. (2013). Influence of peripheral substitution on the magnetic behavior of single-ion magnets based on homo- and heteroleptic Tb^{III} bis(phthalocyaninate). *Chem. Eur. J.* 19 (4): 1457–1465.

68 Rinehart, J.D. and Long, J.R. (2009). Slow magnetic relaxation in a trigonal prismatic uranium(III) complex. *J. Am. Chem. Soc.* 131 (35): 12558–12559.

69 Freedman, D.E., Harman, W.H., Harris, T.D. et al. (2010). Slow magnetic relaxation in a high-spin iron(II) complex. *J. Am. Chem. Soc.* 132 (4): 1224–1225.

70 Zadrozny, J.M., Xiao, D.J., Atanasov, M. et al. (2013). Magnetic blocking in a linear iron(I) complex. *Nat. Chem.* 5 (7): 577–581.

71 Feltham, H.L.C. and Brooker, S. (2014). Review of purely 4f and mixed-metal nd-4f single-molecule magnets containing only one lanthanide ion. *Coord. Chem. Rev.* 276: 1–33.

72 Meihaus, K.R. and Long, J.R. (2015). Actinide-based single-molecule magnets. *Dalton Trans.* 44 (6): 2517–2528.

73 Sun, Y., Takats, J., Eberspacher, T., and Day, V. (1995). Synthesis and structure of tris[dihydrobis(pyrazolyl)borate](tetrahydrofuran)uranium(III), $U[H(\mu\text{-}H)Bpz_2]^3$ (THF): three-center B-H…d U(III) interactions in the presence of coordinated THF ligand. *Inorg. Chim. Acta* 229 (1–2): 315–322.

74 Meihaus, K.R., Minasian, S.G., Lukens, W.W. et al. (2014). Influence of pyrazolate vs N-heterocyclic carbene ligands on the slow magnetic relaxation of homoleptic trischelate lanthanide(III) and uranium(III) complexes. *J. Am. Chem. Soc.* 136 (16): 6056–6068.

75 Coutinho, J.T., Antunes, M.A., Pereira, L.C.J. et al. (2012). Single-ion magnet behaviour in $[U(Tp^{Me2})_2I]$. *Dalton Trans.* 41 (44): 13568–13571.

76 Mills, D.P., Moro, F., McMaster, J. et al. (2011). A delocalized arene-bridged diuranium single-molecule magnet. *Nat. Chem.* 3 (6): 454–460.

77 Moro, F., Mills, D.P., Liddle, S.T., and van Slageren, J. (2013). The inherent single-molecule magnet character of trivalent uranium. *Angew. Chem. Int. Ed.* 52 (12): 3430–3433.

78 King, D.M., Tuna, F., McMaster, J. et al. (2013). Single-molecule magnetism in a single-ion triamidoamine uranium(V) terminal mono-oxo complex. *Angew. Chem. Int. Ed.* 52 (18): 4921–4924.

79 Antunes, M.A., Coutinho, J.T., Santos, I.C. et al. (2015). A mononuclear uranium(IV) single-molecule magnet with an azobenzene radical ligand. *Chem. Eur. J.* 21 (49): 17817–17826.

80 Magnani, N., Apostolidis, C., Morgenstern, A. et al. (2011). Magnetic memory effect in a transuranic mononuclear complex. *Angew. Chem. Int. Ed.* 50 (7): 1696–1698.

81 Magnani, N., Colineau, E., Eloirdi, R. et al. (2010). Superexchange coupling and slow magnetic relaxation in a transuranium polymetallic complex. *Phys. Rev. Lett.* 104 (19): 197202 1–4.

82 Dutkiewicz, M.S., Farnaby, J.H., Apostolidis, C. et al. (2016). Organometallic neptunium(III) complexes. *Nat. Chem.* 8 (8): 797–802.

83 Magnani, N., Colineau, E., Griveau, J.-C. et al. (2014). A plutonium-based single-molecule magnet. *Chem. Commun.* 50 (60): 8171–8173.

84 Mougel, V., Chatelain, L., Pécaut, J. et al. (2012). Uranium and manganese assembled in a wheel-shaped nanoscale single-molecule magnet with high spin-reversal barrier. *Nat. Chem.* 4 (12): 1011–1017.

85 Arnold, P.L., Jones, G.M., Odoh, S.O. et al. (2012). Strongly coupled binuclear uranium–oxo complexes from uranyl oxo rearrangement and reductive silylation. *Nat. Chem.* 4 (3): 221–227.

86 Carretta, S., Amoretti, G., Santini, P. et al. (2013). Magnetic properties and chiral states of a trimetallic uranium complex. *J. Phys. Condens. Matter* 25 (48): 486001 1–6.

87 Arnold, P.L., Hollis, E., Nichol, G.S. et al. (2013). Oxo-functionalization and reduction of the uranyl ion through lanthanide-element bond homolysis: synthetic, structural, and bonding analysis of a series of singly reduced uranyl–rare earth $5f^1$–$4f^n$ complexes. *J. Am. Chem. Soc.* 135 (10): 3841–3854.

88 Mougel, V., Chatelain, L., Hermle, J. et al. (2014). A uranium-based UO_2^+–Mn^{2+} single-chain magnet assembled through cation–cation interactions. *Angew. Chem. Int. Ed.* 53 (3): 819–823.

89 Liddle, S.T. and van Slageren, J. (2015). Improving f-element single molecule magnets. *Chem. Soc. Rev.* 44 (19): 6655–6669.

90 Chatelain, L., Tuna, F., Pécaut, J., and Mazzanti, M. (2015). A zig–zag uranyl(v)–Mn(ii) single chain magnet with a high relaxation barrier. *Chem. Commun.* 51 (56): 11309–11312.

91 Chatelain, L., Pécaut, J., Tuna, F., and Mazzanti, M. (2015). Heterometallic Fe_2^{II}–U^V and Ni_2^{II}–U^V exchange-coupled single-molecule magnets: effect of the 3d ion on the magnetic properties. *Chem. Eur. J.* 21 (50): 18038–18042.

92 Kozimor, S.A., Bartlett, B.M., Rinehart, J.D., and Long, J.R. (2007). Magnetic exchange coupling in chloride-bridged 5f–3d heterometallic complexes generated via insertion into a uranium(IV) dimethylpyrazolate dimer. *J. Am. Chem. Soc.* 129 (35): 10672–10674.

93 Le Borgne, T., Rivière, E., Marrot, J. et al. (2000). Synthesis, crystal structure, and magnetic behavior of linear MUIV complexes (M = Co, Ni, Cu, Zn). *Angew. Chem. Int. Ed.* 39 (9): 1647–1649.

94 Arnold, P.L., Patel, D., Wilson, C., and Love, J.B. (2008). Reduction and selective oxo group silylation of the uranyl dication. *Nature* 451 (7176): 315–317.

95 Monreal, M.J., Carver, C.T., and Diaconescu, P.L. (2007). Redox processes in a uranium bis(1,1′-diamidoferrocene) complex. *Inorg. Chem.* 46 (18): 7226–7228.

96 Layfield, R.A. (2014). Organometallic single-molecule magnets. *Organometallics* 33 (5): 1084–1099.

97 Harriman, K.L.M. and Murugesu, M. (2016). An organolanthanide building block approach to single-molecule magnets. *Acc. Chem. Res.* 49 (6): 1158–1167.

98 Ding, M., Rouzières, M., Losovyj, Y. et al. (2015). Partial nitrogen atom transfer: a new synthetic tool to design single-molecule magnets. *Inorg. Chem.* 54 (18): 9075–9080.

99 Pugh, T., Tuna, F., Ungur, L. et al. (2015). Influencing the properties of dysprosium single-molecule magnets with phosphorus donor ligands. *Nat. Commun.* 6: 7492 1–8.

100 Pugh, T., Vieru, V., Chibotaru, L.F., and Layfield, R.A. (2016). Magneto-structural correlations in arsenic- and selenium-ligated dysprosium single-molecule magnets. *Chem. Sci.* 7 (3): 2128–2137.

101 Tuna, F., Smith, C.A., Bodensteiner, M. et al. (2012). A high anisotropy barrier in a sulfur-bridged organodysprosium single-molecule magnet. *Angew. Chem. Int. Ed.* 51 (28): 6976–6980.

102 Pugh, T., Chilton, N.F., and Layfield, R.A. (2016). A low-symmetry dysprosium metallocene single-molecule magnet with a high anisotropy barrier. *Angew. Chem. Int. Ed.* 55 (37): 11082–11085.

103 Winpenny, R.E.P. (2002). Serendipitous assembly of polynuclear cage compounds. *J. Chem. Soc., Dalton Trans.* (1): 1–10.

104 Aromí, G. and Brechin, E.K. Synthesis of 3d metallic single-molecule magnets. In: *Single-Molecule Magnets and Related Phenomena*, 1–67. Berlin, Heidelberg: Springer-Verlag.

105 Murrie, M. (2010). Cobalt(II) single-molecule magnets. *Chem. Soc. Rev.* 39 (6): 1986–1995.

106 Beltran, L.M.C. and Long, J.R. (2005). Directed assembly of metal–cyanide cluster magnets. *Acc. Chem. Res.* 38 (4): 325–334.

107 Rebilly, J.-N. and Mallah, T. Synthesis of single-molecule magnets using metallocyanates. In: *Single-Molecule Magnets and Related Phenomena*, 103–131. Berlin, Heidelberg: Springer-Verlag.

108 Roubeau, O. and Clérac, R. (2008). Rational assembly of high-spin polynuclear magnetic complexes into coordination networks: the case of a $[Mn_4]$ single-molecule magnet building block. *Eur. J. Inorg. Chem.* 2008 (28): 4325–4342.

109 Tasiopoulos, A.J., Vinslava, A., Wernsdorfer, W. et al. (2004). Giant single-molecule magnets: a $\{Mn_{84}\}$ torus and its supramolecular nanotubes. *Angew. Chem. Int. Ed.* 43 (16): 2117–2121.

110 Moushi, E.E., Stamatatos, T.C., Wernsdorfer, W. et al. (2009). A Mn_{17} octahedron with a giant ground-state spin: occurrence in discrete form and as multidimensional coordination polymers. *Inorg. Chem.* 48 (12): 5049–5051.

111 Cremades, E. and Ruiz, E. (2010). Magnetic properties of largest-spin single molecule magnets: Mn_{17} complexes—a density functional theory approach. *Inorg. Chem.* 49 (20): 9641–9648.

112 Ruiz, E., Cirera, J., Cano, J. et al. (2008). Can large magnetic anisotropy and high spin really coexist? *Chem. Commun.* (1): 52–54.

113 Waldmann, O. (2007). A criterion for the anisotropy barrier in single-molecule magnets. *Inorg. Chem.* 46 (24): 10035–10037.

114 Neese, F. and Pantazis, D.A. (2011). What is not required to make a single molecule magnet. *Faraday Discuss.* 148 (0): 229–238.

115 Wernsdorfer, W. (2001). Classical and quantum magnetization reversal studied in nanometer-sized particles and clusters. *Adv. Chem. Phys.* 118: 99–190.

116 Wernsdorfer, W. and Sessoli, R. (1999). Quantum phase interference and parity effects in magnetic molecular clusters. *Science* 284 (5411): 133–135.

117 Glaser, T. (2011). Rational design of single-molecule magnets: a supramolecular approach. *Chem. Commun.* 47 (1): 116–130.

118 Mitchell, K.J., Abboud, K.A., and Christou, G. (2016). Magnetostructural correlation for high-nuclearity iron(III)/oxo complexes and application to Fe_5, Fe_6, and Fe_8 clusters. *Inorg. Chem.* 55 (13): 6597–6608.

119 Aravena, D., Venegas-yazigi, D., and Ruiz, E. (2016). Single-molecule magnet properties of transition-metal ions encapsulated in lacunary polyoxometalates: a theoretical study. *Inorg. Chem.* 55 (13): 6405–6413.

120 Sato, R., Suzuki, K., Minato, T. et al. (2015). Field-induced slow magnetic relaxation of octahedrally coordinated mononuclear Fe(III)-, Co(II)-, and Mn(III)-containing polyoxometalates. *Chem. Commun.* 51: 4081–4084.

121 Pointillart, F., Bernot, K., Golhen, S. et al. (2015). Magnetic memory in an isotopically enriched and magnetically isolated mononuclear dysprosium complex. *Angew. Chem. Int. Ed.* 54 (5): 1504–1507.

122 Benioff, P. (1982). Quantum mechanical Hamiltonian models of Turing machines. *J. Stat. Phys.* 29 (3): 515–546.

123 Pedersen, K.S., Ariciu, A.-M., McAdams, S. et al. (2016). Toward molecular 4f single-ion magnet qubits. *J. Am. Chem. Soc.* 138 (18): 5801–5804.

124 Sessoli, R. (2015). Toward the quantum computer: magnetic molecules back in the race. *ACS Cent. Sci.* 1 (9): 473–474.

125 Fatila, E.M., Rouzières, M., Jennings, M.C. et al. (2013). Fine-tuning the single-molecule magnet properties of a $[Dy(III)\text{-radical}]_2$ pair. *J. Am. Chem. Soc.* 135 (26): 9596–9599.

126 Atzori, M., Tesi, L., Morra, E. et al. (2016). Room-temperature quantum coherence and rabi oscillations in vanadyl phthalocyanine: toward multifunctional molecular spin qubits. *J. Am. Chem. Soc.* 138 (7): 2154–2157.

127 Fataftah, M.S., Zadrozny, J.M., Coste, S.C. et al. (2016). Employing forbidden transitions as qubits in a nuclear spin-free chromium complex. *J. Am. Chem. Soc.* 138 (4): 1344–1348.

128 Leuenberger, M.N. and Loss, D. (2001). Quantum computing in molecular magnets. *Nature* 410 (6830): 789–793.

129 Song, Y. (2009). *High Density Data Storage, Principle, Technology, and Materials*. Singapore: World Scientific.

130 Luis, F., Repollés, A., Martínez-Pérez, M.J. et al. (2011). Molecular prototypes for spin-based CNOT and SWAP quantum gates. *Phys. Rev. Lett.* 107 (11): 117203-1–117203-5.

131 Kiefl, E., Mannini, M., Bernot, K. et al. (2016). Robust magnetic properties of a sublimable single-molecule magnet. *ACS Nano* 10 (6): 5663–5669.

132 Wäckerlin, C., Donati, F., Singha, A. et al. (2016). Giant hysteresis of single-molecule magnets adsorbed on a nonmagnetic insulator. *Adv. Mater.* 28 (26): 5195–5199.

133 Zu, F.-X., Gao, G.-Y., Fu, H.-H. et al. (2015). Efficient spin filter and spin valve in a single-molecule magnet Fe_4 between two graphene electrodes. *Appl. Phys. Lett.* 107 (25): 252403 1–4.

134 del Carmen Giménez-López, M., Moro, F., La Torre, A. et al. (2011). Encapsulation of single-molecule magnets in carbon nanotubes. *Nat. Commun.* 2: 407 1–6.

135 Nakanishi, R., Yatoo, M.A., Katoh, K. et al. (2017). Dysprosium acetylacetonato single-molecule magnet encapsulated in carbon nanotubes. *Materials* 10: 7. doi: 10.3390/ma10010007 1–8.

136 Wu, J., Zhao, L., Zhang, L. et al. (2016). Macroscopic structures macroscopic hexagonal tubes of 3d–4f metallocycles. *Angew. Chem. Int. Ed.* 15574–15578.

137 Geim, A.K. and Novoselov, K.S. (2007). The rise of graphene. *Nat. Mater.* 6 (3): 183–191.

138 Lumetti, S., Candini, A., Godfrin, C. et al. (2016). Single-molecule devices with graphene electrodes. *Dalton Trans.* 45 (42): 16570–16574.

139 Islam, F. and Benjamin, C. (2016). Adiabatically twisting a magnetic molecule to generate pure spin currents in graphene. *J. Phys. Condens. Matter.* 28 (3): 035305 1–9.

140 Dreiser, J., Pacchioni, G.E., Donati, F. et al. (2016). Out-of-plane alignment of Er(trensal) easy magnetization axes using graphene. *ACS Nano* 10 (2): 2887–2892.

141 Fetoh, A., Cosquer, G., Morimoto, M. et al. (2016). Photo-activation of single molecule magnet behavior in a manganese-based complex. Nat. Publ. Gr., (February), 1–6. *Sci. Rep.* 6: 23785 1–6.

142 Microarrays, M., Serri, M., Mannini, M. et al. (2017). Low-temperature magnetic force microscopy on single molecule magnet-based microarrays. *Nano Lett.* 17 (3): 1899–1905.

143 Evangelisti, M. and Brechin, E.K. (2010). Recipes for enhanced molecular cooling. *Dalton Trans.* 39 (20): 4672–4676.

144 Mondal, A.K., Jena, H.S., Malviya, A., and Konar, S. (2016). Lanthanide-directed fabrication of four tetranuclear quadruple stranded helicates showing magnetic refrigeration and slow magnetic relaxation. *Inorg. Chem.* 55 (11): 5237–5244.

145 Evangelisti, M., Candini, A., Ghirri, A. et al. (2005). Spin-enhanced magnetocaloric effect in molecular nanomagnets. *Appl. Phys. Lett.* 87 (7): 072504 1–3.

146 Shaw, R., Laye, R.H., Jones, L.F. et al. (2007). 1,2,3-Triazolate-bridged tetradecametallic transition metal clusters $[M_{14}(L)_6O_6(OMe)_{18}X_6](M = Fe^{III}$, Cr^{III} and $V^{III/IV})$ and related compounds: ground-state spins ranging from $S = 0$ to $S = 25$ and spin-enhanced magnetocaloric effect. *Inorg. Chem.* 46 (12): 4968–4978.

147 Low, D.M., Jones, L.F., Bell, A. et al. (2003). Solvothermal synthesis of a tetradecametallic Fe^{III} cluster. *Angew. Chem. Int. Ed.* 42 (32): 3781–3784.

148 Manoli, M., Johnstone, R.D.L., Parsons, S. et al. (2007). A ferromagnetic mixed-valent Mn supertetrahedron: towards low-temperature magnetic refrigeration with molecular clusters. *Angew. Chem. Int. Ed.* 46 (24): 4456–4460.

149 Manoli, M., Collins, A., Parsons, S. et al. (2008). Mixed-valent Mn supertetrahedra and planar discs as enhanced magnetic coolers. *J. Am. Chem. Soc.* 130 (33): 11129–11139.

150 Wang, W.-M., Zhang, H.-X., Wang, S.-Y. et al. (2015). Ligand field affected single-molecule magnet behavior of lanthanide(III) dinuclear complexes with an 8-hydroxyquinoline Schiff base derivative as bridging ligand. *Inorg. Chem.* 54 (22): 10610–10622.

151 Karotsis, G., Kennedy, S., Teat, S.J. et al. (2010). $[Mn^{III}_4Ln^{III}_4]$Calix[4]arene clusters as enhanced magnetic coolers and molecular magnets. *J. Am. Chem. Soc.* 132 (37): 12983–12990.

152 Pedersen, K.S., Lorusso, G., Morales, J.J. et al. (2014). Fluoride-bridged $\{Gd^{III}_3M^{III}_2\}$ (M = Cr, Fe, Ga) molecular magnetic refrigerants. *Angew. Chem. Int. Ed.* 53 (9): 2394–2397.

153 Peng, J., Kong, X., Zhang, Q. et al. (2014). Beauty, symmetry, and magnetocaloric effect—four-shell keplerates with 104 lanthanide atoms. *J. Am. Chem. Soc.* 104: 20–23.

154 Corradini, V., Ghirri, A., Candini, A. et al. (2013). Magnetic cooling at a single molecule level: a spectroscopic investigation of isolated molecules on a surface. *Adv. Mater.* 25 (20): 2816–2820.

155 Lorusso, G., Roubeau, O., and Evangelisti, M. (2016). Rotating magnetocaloric effect in an anisotropic molecular dimer. *Angew. Chem. Int. Ed.* 55 (10): 3360–3363.

156 Balli, M., Jandl, S., Fournier, P., and Gospodinov, M.M. (2014). Anisotropy-enhanced giant reversible rotating magnetocaloric effect in $HoMn_2O_5$ single crystals. *Appl. Phys. Lett.* 104 (23): 232402.

157 Tkáč, V., Orendáčová, A., Čižmár, E. et al. (2015). Giant reversible rotating cryomagnetocaloric effect in $KEr(MoO_4)_2$ induced by a crystal-field anisotropy. *Phys. Rev. B* 92 (2): 024406 1–5.

158 Wu, J., Li, X., Zhao, L. et al. (2017). Enhancement of Magnetocaloric effect through fixation of carbon dioxide: molecular assembly from Ln_4 to Ln_4 cluster pairs. *Inorg. Chem.* 56 (7): 4104–4111.

159 Kim, B., Schmieder, A.H., Stacy, A.J. et al. (2012). Sensitive biological detection with a soluble and stable polymeric paramagnetic nanocluster. *J. Am. Chem. Soc.* 134 (25): 10377–10380.

160 Mertzman, J.E., Kar, S., Lofland, S. et al. (2009). Surface attached manganese–oxo clusters as potential contrast agents. *Chem. Commun.* (7): 788–790.

161 Wang, Y., Li, W., Zhou, S. et al. (2011). Mn_{12} single-molecule magnet aggregates as magnetic resonance imaging contrast agents. *Chem. Commun.* 47 (12): 3541–3543.

162 Alexandropoulos, D.I., Fournet, A., Cunha-Silva, L. et al. (2016). "Molecular nanoclusters": a 2-nm-sized $\{Mn_{29}\}$ cluster with a spherical structure. *Inorg. Chem.* 5523: 12118–12121.

163 Jiang, X., Liu, C.-M., and Kou, H.-Z. (2016). Porous coordination polymers based on $\{Mn_6\}$ single-molecule magnets. *Inorg. Chem.* 55 (12): 5880–5885.

164 Pointillart, F., le Guennic, B., Cador, O. et al. (2015). Lanthanide ion and tetrathiafulvalene-based ligand as a "magic" couple toward luminescence,

single molecule magnets, and magnetostructural correlations. *Acc. Chem. Res.* 48 (11): 2834–2842.

165 Gao, H.-L., Jiang, L., Wang, W.-M. et al. (2016). Single-molecule-magnet behavior and fluorescence properties of 8-hydroxyquinolinate derivative-based rare-earth complexes. *Inorg. Chem.* 55 (17): 8898–8904.

166 Pinkowicz, D., Ren, M., Zheng, L.-M. et al. (2014). Control of the single-molecule magnet behavior of lanthanide-diarylethene photochromic assemblies by irradiation with light. *Chem. Eur. J.* 20 (39): 12502–12513.

167 Bi, Y., Chen, C., Zhao, Y.-F. et al. (2016). Thermostability and photoluminescence of Dy(III) single-molecule magnets under a magnetic field. *Chem. Sci.* 7 (8): 5020–5031.

168 Salomon, W., Lan, Y., Yang, S. et al. (2016). Single-molecule magnet behavior of individual polyoxometalate molecules incorporated within biopolymer or metal–organic framework matrices. *Chemistry* 22: 6564–6574.

169 Vallejo, J., Pardo, E., Viciano-Chumillas, M. et al. (2017). Reversible solvato-magnetic switching in a single-ion magnet from an entatic state. *Chem. Sci.* 8: 3694–3702.

170 Ou-Yang, J.-K., Saleh, N., Fernandez Garcia, G. et al. (2016). Improved slow magnetic relaxation in optically pure helicene-based Dy^{III} single molecule magnets. *Chem. Commun.* 52 (100): 14474–14477.